J|A|C|S
ARTICLES
Published on Web 07/18/2002

Dimerization of Merocyanine Dyes. Structural and Energetic Characterization of Dipolar Dye Aggregates and Implications for Nonlinear Optical Materials

Frank Würthner,*[,†] Sheng Yao,[†,§] Tony Debaerdemaeker,[‡] and Rüdiger Wortmann*[,§]

Contribution from the Department of Organic Chemistry II and the Section of Crystallography, University of Ulm, Albert-Einstein-Allee 11, D-89081 Ulm, Germany, and Department of Physical Chemistry, University of Kaiserslautern, Erwin-Schrödinger-Strasse, D-67663 Kaiserslautern, Germany

Received February 1, 2002

Abstract: Aggregation of polar merocyanine dyes has been identified as an important problem in the fabrication of organic materials for photonic applications. In this work, a series of merocyanine dyes is synthesized, and their aggregation is investigated by a combination of several experimental techniques to reveal structure−property relationships. These studies provide clear evidence for the formation of centrosymmetric dimers for all investigated merocyanines in concentrated solution and in the solid state. The thermodynamics of dimerization in liquid solution is studied by concentration-dependent permittivity measurements, UV−vis spectroscopy, and electrooptical absorption experiments. A centrosymmetric dimer structure with antiparallel ordering of the dipole moments is observed in solution by 2D NMR spectroscopy as well as in the solid state by X-ray crystallography and interpreted in terms of dipolar and $\pi-\pi$ interactions. The optical properties of the dimer aggregates are satisfactorily explained by an excitonic coupling model. The effect of an external electric field on the dimerization equilibrium is considered and quantitatively determined by electrooptical absorption measurements. Implications of the observed findings on the design of nonlinear optical and photorefractive materials are discussed.

Introduction

Organic materials for nonlinear optical (NLO)[1] and photorefractive (PR)[2] applications rely on a noncentrosymmetric ordering of dye molecules. A number of different techniques have been utilized to achieve this ordering, including crystallization in asymmetric space groups,[3] preparation of asymmetric thin films by Langmuir−Blodgett and self-assembly techniques,[4] and poling of polymer-dissolved or polymer-attached dipolar dyes by strong external electric fields.[5−9] The latter method may be applied to amorphous materials and thus allows particularly convenient preparation of thin films with varying thicknesses and geometries. Acentric second-order NLO materials with nonpolar order have also been described[1d,4d] but will not be discussed in this paper.

* To whom correspondence should be addressed. E-mail: frank.wuerthner@chemie.uni-ulm.de, ruediger.wortmann@chemie.uni-kl.de.
† Organic Chemistry II, University of Ulm.
‡ Section of Crystallography, University of Ulm.
§ Physical Chemistry, University of Kaiserslautern.

(1) Review articles: (a) Zyss, J., Ed. *Molecular Nonlinear Optics: Materials, Physics, Devices*; Academic Press: Boston, MA, 1994. (b) Nalwa, H. S., Miyata, S., Eds. *Nonlinear Optics of Organic Molecules and Polymers*; CRC Press: Boca Raton, FL, 1997. (c) Prasad, P. N.; Williams, D. J. *Introduction to Nonlinear Optical Effects in Molecules and Polymers*; John Wiley: New York, 1991. (d) Wolff, J. J.; Wortmann, R. *Adv. Phys. Org. Chem.* **1999**, *32*, 121−217. (e) Verbiest, T.; Houbrechts, S.; Kauranen, M.; Clays, K.; Persoons, A. *J. Mater. Chem.* **1997**, *7*, 2175−2189. (f) Kanis, D. R.; Ratner, M. A.; Marks, T. J. *Chem. Rev.* **1994**, *94*, 195−242. (g) Marder, S. R.; Perry, J. W. *Adv. Mater.* **1993**, *5*, 804−815. (h) Marks, T. J.; Ratner, M. A. *Angew. Chem., Int. Ed. Engl.* **1995**, *34*, 155−175. (i) Ma, H.; Jen, A. K.-Y. *Adv. Mater.* **2001**, *13*, 1201−1205.

(2) Review articles: (a) Moerner, W. E.; Silence, S. M. *Chem. Rev.* **1994**, *94*, 127−155. (b) Zhang, Y.; Burzynski, R.; Ghosal, S.; Casstevens, M. K. *Adv. Mater.* **1996**, *8*, 111−125. (c) Moerner, W. E.; Grunnet-Jepsen, A.; Thompson, C. L. *Annu. Rev. Mater. Sci.* **1997**, *27*, 585−623. (d) Zilker, S. *Chem. Phys. Chem.* **2000**, *1*, 72−87. (e) Würthner, F.; Wortmann, R.; Meerholz, K. *Chem. Phys. Chem.* **2001**, *3*, 17−31.

(3) (a) Marder, S. R.; Perry, J. W.; Yakymyshyn, C. P. *Chem. Mater.* **1994**, *6*, 1137. (b) Zyss, J.; Nicoud, M.; Coquillay, J. *J. Chem. Phys.* **1984**, *81*, 4160. (c) Evans, C. E.; Bagieu-Beucher, M.; Masse, R.; Nicoud, J. F. *Chem. Mater.* **1998**, *10*, 847. (d) Wong, M. S.; Meier, U.; Pan, F.; Gramlich, V.; Bosshard, C.; Günter, P. *Adv. Mater.* **1996**, *8*, 416−420.

(4) (a) Yitzchaik, S.; Marks, T. J. *Acc. Chem. Res.* **1996**, *29*, 197−202. (b) Pan, F.; Wong, M. S.; Gramlich, V.; Bosshard, C.; Günter, P. *J. Am. Chem. Soc.* **1996**, *118*, 6315−6316. (c) Cai, C.; Bösch, M. M.; Tao, Y.; Müller, B.; Gan, Z.; Kündig, A.; Bosshard, C.; Liakatas, I.; Jäger, M.; Günter, P. *J. Am. Chem. Soc.* **1998**, *120*, 8563−8564. (d) Ashwell, G. J. *J. Mater. Chem.* **1999**, *9*, 1991−2003. (e) Yang, X.; McBranch, D.; Swanson, B.; Li, D. *Angew. Chem., Int. Ed. Engl.* **1996**, *35*, 538−540.

(5) Review articles: (a) Burland, D. M.; Miller, R. D.; Walsh, C. A. *Chem. Rev.* **1994**, *94*, 31−75. (b) Dalton, L. R.; Steier, W. H.; Robinson, B. H.; Zhang, C.; Ren, A.; Garner, S.; Chen, A.; Londergan, T.; Irwin, L.; Carlson, B.; Fifield, L.; Phelan, G.; Kincaid, C.; Amend, J.; Jen, A. *J. Mater. Chem.* **1999**, *9*, 1905−1920. (c) Ulrich, D. R. *Mol. Cryst. Liq. Cryst.* **1988**, *160*, 1−31. (d) Twieg, R. J.; Dirk, C. W. In *Science and Technology of Organic Thini Films for Waveguiding Nonlinear Optics*; Kajzar, F., Swalen, J., Eds.; Gordon Breach: Amsterdam, 1996.

(6) (a) Ahlheim, M.; Barzoukas, M.; Bedworth, P. V.; Blanchard-Desce, M.; Fort, A.; Hu, Z.-Y.; Marder, S. R.; Perry, J.; Runser, C.; Staehlin, M.; Zysset, B. *Science* **1996**, *271*, 335−337. (b) Marder, S. R.; Gorman, C. B.; Tiemann, B. G.; Cheng, L.-T. *J. Am. Chem. Soc.* **1993**, *115*, 3006−3007.

(7) Verbiest, T.; Burland, D. M.; Jurich, C.; Lee, U. Y.; Miller, R. D.; Volksen, W. *Science* **1995**, *268*, 1604−1606.

(8) (a) Wu, X.; Wu, J.; Jen, A. K.-Y. *J. Am. Chem. Soc.* **1999**, *121*, 472−473. (b) Shu, C.-F.; Tsai, W.-J.; Jen, A. K.-Y. *Tetrahedron Lett.* **1996**, *37*, 7055−7058.

(9) (a) Dalton, L. R.; Harper, A. W.; Robinson, B. H. *Proc. Natl. Acad. Sci. U.S.A.* **1997**, *94*, 4842−4847. (b) Robinson, B. H.; Dalton, L. R.; Harper, A. W.; Ren, A.; Wang, F.; Zhang, C.; Todorova, G.; Lee, M.; Aniszfeld, R.; Garner, S.; Chen, A.; Steier, W. H.; Houbrecht, S.; Persoons, A.; Ledoux, I.; Zyss, J.; Jen, A. K. Y. *Chem. Phys.* **1999**, *245*, 35−50.

Research on poled materials initially focused on the molecular figures-of-merit (FOMs) of the electrooptical chromophores, and significant progress could be reached in understanding the relationships between (non)linear polarizabilities and the structures of the π-conjugated systems.[10,11] The molecular FOM for second-order nonlinear optical materials was shown to depend on the dipole moment μ and the second-order polarizability β, while the FOM of organic PR materials with low glass transition temperature was demonstrated to be governed mainly by the dipole moment and the anisotropy of the linear polarizability, $\delta\alpha$.[12] Due to the tunability of the π-system of merocyanines from weakly dipolar (polyene-like) to highly dipolar (zwitterionic) chromophores, merocyanines were identified as the most promising chromophore structures to optimize the respective molecular FOMs.[10,13−15] Important research was also carried out on alternative donor−acceptor substituted π-systems such as stilbenes,[16] oligothiophenes,[17] and other dyes.[18,19]

In the process of device development, however, many materials based on well-designed chromophores with large dipole moments and excellent (hyper)polarizabilities failed to provide the expected electrooptic response.[20] This malfunction was clearly related to the high dye concentration required in the polymeric composites and was attributed to the formation of dye aggregates. In 1997, Dalton, Marks, and others succeeded in providing experimental evidence that electrostatic intermolecular interactions between the dye molecules accounted for the observed deficiencies.[9,21,22] This work pinpointed the ambiguous nature of the dipolarity of the dyes. On the one hand, large dipole moments are required to achieve noncentrosymmetry by poling in external electric fields. On the other hand, the dipole moments lead to strong intermolecular interaction and to formation of inactive aggregates at higher dye loading. A centrosymmetric structure of the dye aggregates in amorphous materials[9,21,22] was clearly suggested by the nature of the electrostatic interactions but was not experimentally proven until recently.[23,24] A centrosymmetric (antiparallel) dimer structure also explained the discrepancies between the observed electrooptical effects of polymeric composite materials at high dye loading and the predicted effects based on molecular FOMs experimentally determined from NLO experiments on dilute solutions.

Similar problems were also encountered in the development of organic PR materials which require dyes of even higher dipolarity than second-order NLO applications.[12,14] We recently achieved significant improvements in the refractive index modulation efficiencies of such materials based on merocyanine dyes following design strategies suggested by the corresponding molecular FOM.[14,15,25] Despite the excellent PR performance, there was also evidence for partial dye aggregation in materials based on the chromophoric system of dyes **2** (ATOP).[14,26] Notably, for dyes **1**, which exhibit an even higher molecular PR FOM due to a significantly larger dipole moment, aggregation prevented the realization of any reasonable material at all. The materials either crystallized or remained amorphous but did not show any PR response. These rather drastic deviations from the FOM predictions triggered our interest in elucidating the structural and energetic origin of the strong intermolecular interactions between the dye molecules. In a first step, we investigated the highly dipolar dyes **1a**−**m** bearing substituents of different bulkiness.[23] Now we demonstrate that the observations for the highly dipolar dyes **1a**−**m** may be generalized to a common description of merocyanine dimerization by dipolar interactions. A representative selection of merocyanine dyes has been investigated to identify common structure−property relationships using several experimental techniques, including permittivity measurements, UV−vis spectroscopy, electrooptical absorption measurements (EOAM), 2D NMR spectroscopy, and X-ray crystallography. The optical properties of the dimer aggregates are explained in terms of an excitonic coupling model. We also present experimental results on the influence of an external electric field on the dimerization equilibrium and an interpretation of this effect. Implications of these findings

(10) (a) Marder, S. R.; Gorman, C. B.; Meyers, F.; Perry, J. W.; Bourhill, G.; Brédas, J.-L.; Pierce, B. M. *Science* **1994**, *265*, 632−635. (b) Marder, S. R.; Cheng, L.-T.; Tiemann, B. G.; Friedli, A. C.; Blanchard-Desce, M.; Perry, J. W.; Skindoj, J. *Science* **1994**, *263*, 511−514. (c) Marder, S. R.; Gorman, C. B.; Tienmann, B. G.; Cheng, L.-T. *J. Am. Chem. Soc.* **1993**, *115*, 3006−3007.

(11) Oudar, J. L.; Chemla, D. S. *J. Chem. Phys.* **1977**, *66*, 2664−2668.

(12) Wortmann, R.; Poga, C.; Twieg, R. J.; Geletneky, C.; Moylan, C. R.; Lundquist, P. M.; DeVoe, R. G.; Cotts, P. M.; Horn, H.; Rice, J.; Burland, D. M. *J. Chem. Phys.* **1996**, *105*, 10637−10647.

(13) (a) Blanchard-Desce, M.; Ledoux, I.; Lehn, J.-M.; Malthête, J.; Zyss, J. *J. Chem. Soc., Chem. Commun.* **1988**, 737. (b) Blanchard-Desce, M.; Alain, V.; Bedworth, P. V.; Marder, S. R.; Fort, A.; Runser, C.; Barzoukas, M.; Lebus, S.; Wortmann, R. *Chem. Eur. J.* **1997**, *3*, 1091−1104. (c) Blanchard-Desce, M.; Alain, V.; Midrier, L.; Wortmann, R.; Lebus, S.; Glania, C.; Krämer, P.; Fort, A.; Muller, J.; Barzoukas, M. *J. Photochem. Photobiol.* **1997**, *105*, 115−121. (d) Cabrera, I.; Althoff, O.; Man, H.-T.; Yoon, H. N. *Adv. Mater*. **1994**, *6*, 43−45.

(14) Würthner, F.; Wortmann, R.; Matschiner, R.; Lukaszuk, K.; Meerholz, K.; DeNardin, Y.; Bittner, R.; Bräuchle, C.; Sens, R. *Angew. Chem., Int. Ed. Engl.* **1997**, *36*, 2765−2768.

(15) (a) Wortmann, R.; Würthner, F.; Sautter, A.; Lukaszuk, K.; Matschiner, R.; Meerholz, K. *Proc. SPIE* **1998**, *3471*, 41−49. (b) Beckmann, S.; Etzbach, K.-H.; Krämer, P.; Lukaszuk, K.; Matschiner, R.; Schmidt, A. J.; Schuhmacher, P.; Sens, R.; Seybold, G.; Wortmann, R.; Würthner, F. *Adv. Mater*. **1999**, *11*, 536−541.

(16) (a) Jen, A. K.-Y.; Rao, P.; Wong, K. Y.; Drost, K. J. *J. Chem. Soc., Chem. Commun*. **1993**, 90−91. (b) Wu, X.; Wu, J.; Liu, Y.; Jen, A. K.-Y. *Chem. Commun*. **1999**, 2391−2392. (c) Cheng, L.-T.; Wilson, T.; Stevenson, S. H.; Meredith, G. R.; Rikken, G.; Marder, S. R. *J. Phys. Chem.* **1991**, *95*, 10631−10643.

(17) (a) Würthner, F.; Effenberger, F.; Wortmann, R.; Krämer, P. *Chem. Phys*. **1993**, 173, 305−314. (b) Steybe, F.; Effenberger, F.; Beckmann, S.; Krämer, P.; Glania, C.; Wortmann, R. *Chem. Phys.* **1997**, *219*, 317−331. (c) Hutchings, M. G.; Feguson, I.; McGeein, D. J.; Morley, J. O.; Zyss, J.; Ledoux, I. *J. Chem. Soc., Perkin Trans. 2* **1995**, 171−180.

(18) (a) Cheng, L.-T.; Wilson, T.; Marder, S. R.; Stiegman, A. E.; Rikken, G.; Spangler, C. W. *J. Phys. Chem.* **1991**, *95*, 10643−10652. (b) Dirk, C. W.; Katz, H. E.; Schilling, M. L.; King, L. A. *Chem. Mater*. **1990**, *2*, 700.

(19) (a) Long, N. J. *Angew. Chem., Int. Ed. Engl*. **1995**, *34*, 6. (b) LeCours, S. M.; Guan, H.-W.; DiMagno, S. G.; Wang, C. H.; Therien, M. J. *J. Am. Chem. Soc*. **1996**, *118*, 1497.

(20) (a) Dörr, M.; Zentel, R.; Dietrich, R.; Meerholz, K.; Bräuchle, C.; Wichern, J.; Zippel, S.; Boldt, P. *Macromolecules* **1998**, *31*, 1454−1465. (b) Hagen, R.; Zobel, O.; Sahr, O.; Biber, M.; Eckl, M.; Strohriegl, P.; Eisenbach, C.-D.; Haarer, D. *J. Appl. Phys.* **1996**, *80*, 3162−3166. (c) It may be assumed that numerous work has not been published if aggregation led to completely inactive materials. This was also the case for a number of polymers based on azo and methine dyes in our own earlier work.

(21) (a) Yitzchaik, S.; Di Bella, S.; Lundquist, P. M.; Wong, G. K.; Marks, T. J. *J. Am. Chem. Soc.* **1997**, *119*, 2995−3002. (b) Di Bella, S.; Fragalà, I.; Marks, T. J.; Ratner, M. A. *J. Am. Chem. Soc.* **1996**, *118*, 12747−12751.

(22) Van der Vorst, C. P. J. M.; Picken, S. J. In *Polymers as electrooptical and photooptical active media*; Shibaev, V. P., Ed.; Springer-Verlag: Berlin, 1996; pp 173−211.

(23) Würthner, F.; Yao, S. *Angew. Chem., Int. Ed.* **2000**, *39*, 1978−1981.

(24) For recent interesting work on merocyanines and hemicyanine dye aggregates in Langmuir−Blodgett films, see ref 4d and the following: (a) Ashwell, G. J.; Skjonnemand, K.; Paxton, G. A. N.; Allen, D. W.; Mifflin, J. P. L.; Li, X. *J. Mater. Chem.* **2001**, *11*, 1351−1356. (b) Ricceri, R.; Neto, C; Abbotto, A.; Facchetti, A.; Pagani, G. A. *Langmuir* **1999**, *15*, 2149−2151. For tethered mero- and hemicyanines which afford intramolecular dye dimers, see: (c) Lu, L.; Lachicotte, R. J.; Penner, T. L.; Perlstein, J.; Whitten, D. G. *J. Am. Chem. Soc.* **1999**, *121*, 8414−8156. (d) Katoh, T.; Inagaki, Y.; Okazaki, R. *J. Am. Chem. Soc.* **1998**, *120*, 3623−3628. (e) Zeena, S.; Thomas, G. K. *J. Am. Chem. Soc.* **2000**, *123*, 7859−7865. (f) Ushakov, E. N.; Gromov, S. P.; Federova, O. A.; Pershina, Y. V.; Alfimov, M. V.; Barigelletti, F.; Flamigni, L.; Balzani, V. *J. Phys. Chem. A* **1999**, *50*, 11189−11193.

(25) (a) Würthner, F.; Thalacker, C.; Matschiner, R.; Lukaszuk, K.; Wortmann, R. *Chem. Commun.* **1998**, 1739−1740.

(26) Meerholz, K.; DeNardin, Y.; Bittner, R.; Wortmann, R.; Würthner, F. *Appl. Phys. Lett.* **1998**, *73*, 4−6.

Chart 1

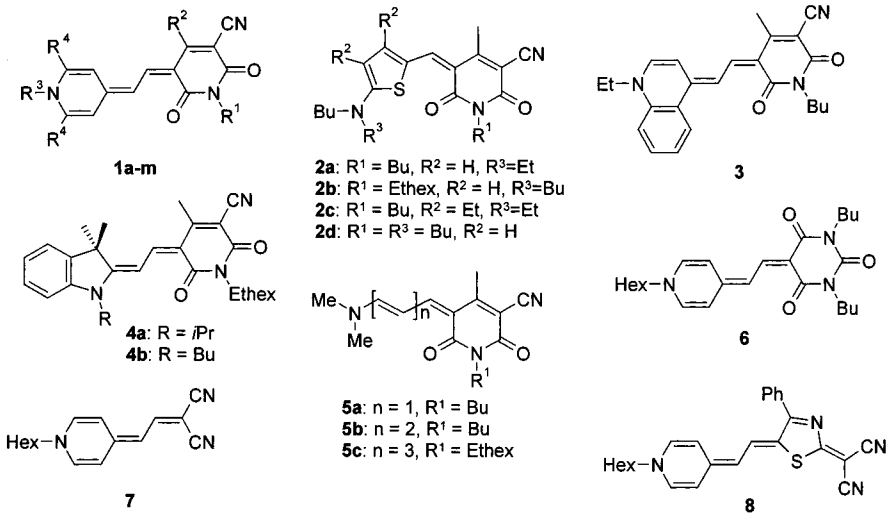

Scheme 1. Synthesis of Dyes **1a**−**m**[a]

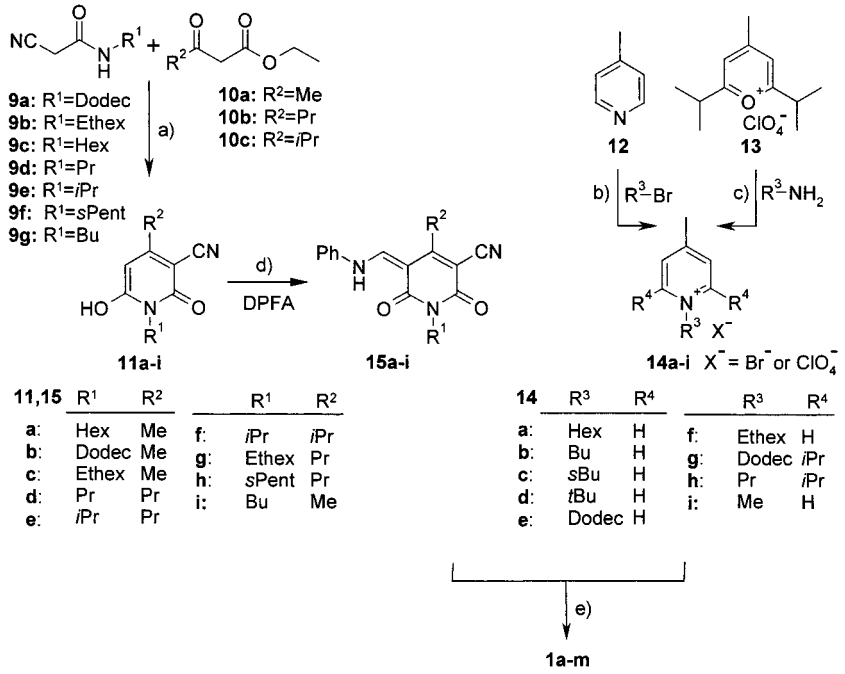

11,15	R¹	R²		R¹	R²
a:	Hex	Me	**f**:	*i*Pr	*i*Pr
b:	Dodec	Me	**g**:	Ethex	Pr
c:	Ethex	Me	**h**:	*s*Pent	Pr
d:	Pr	Pr	**i**:	Bu	Me
e:	*i*Pr	Pr			

14	R³	R⁴		R³	R⁴
a:	Hex	H	**f**:	Ethex	H
b:	Bu	H	**g**:	Dodec	*i*Pr
c:	*s*Bu	H	**h**:	Pr	*i*Pr
d:	*t*Bu	H	**i**:	Me	H
e:	Dodec	H			

[a] Conditions: (a) piperidine/NaOH, 100 °C, 20 h, yield 5−59%. (b) EtOH or 2-propanol, reflux, 10 h. (c) Et_3N, CH_2Cl_2, room temperature 10 h, yield 51−62%. (d) Ac_2O, room temperature 15−30 min, 90 °C, 5−15 min. (e) Ac_2O, 90 °C, 2−20 h, yield 32−90%. DPFA = *N*,*N*′-diphenylformamidine, Ethex = *rac*-2-ethylhexyl, *s*Pent = *rac*-1-methylbutyl. The substituents of **1a**−**m** are defined in Table 1.

on the design and implementation of NLO and PR materials are discussed.

Results

Synthesis. The structures of the dyes are presented in Chart 1. The structural variation of dyes **1a**−**m** was accomplished according to Scheme 1. Hydroxypyridones **11a**−**i** were obtained by a sequence of condensation reactions in which first cyanoacetic acid amides **9a**−**g** were prepared in situ from ethyl cyanoacetate and the respective amine, and subsequent reaction with acyl acetates **10a**−**c** afforded **11a**−**i**.[27] This one-pot synthesis is straightforward and the yields are acceptable, as long as no sterically demanding group is involved at position R^2. However, in the case of **11f**, which bears a secondary alkyl group at R^2, the reaction was achieved only in the presence of a strong base (e.g., NaOH) and in low yields (5%). 4-Picoline derivatives **14a**−**i** were obtained by S_N1 and S_N2 alkylation of **12** or by nucleophilic amination of **13**. Reaction of **11a**−**i** with *N*,*N*′-diphenylformamidine in acetic anhydride afforded enaminones **15a**−**i**,[28] which could be reacted in situ with **14a**−**i** to give merocyanine dyes **1a**−**m** (Table 1) in moderate to high yields.

On a smaller scale, some variations of the sterical demand have also been applied for dyes **2a**−**d** and **4a**,**b**, whose accessibility has already been described.[14,28] Only for the introduction of the ethyl groups at the 3,4 positions of the thiophene unit did some additional synthetic steps become

(27) (a) Guareschi, J. *Ber. Dtsch. Chem. Ges. Board 4 (Referate, Patente, Nekrologe)* **1896**, *29*, 654−656. (b) Bello, K. A. *Dyes Pigm.* **1995**, *28*, 83−90. (c) Katritzky, A. R.; Rachwal, S.; Smith, T. J. *Heterocycl. Chem.* **1995**, *32*, 1007−1010.

(28) (a) Würthner, F.; Sens, R.; Etzbach, K.-H.; Seybold, G. *Angew. Chem., Int. Ed.* **1999**, *38*, 1649−1652. (b) Würthner, F. *Synthesis* **1999**, 2103−2113. (c) Würthner, F.; Yao, S.; Wortmann, R. *J. Inf. Rec.* **2000**, *25*, 69−86.

Table 1. Absorption Maxima λ, Dimerization Constants K_{dim}, Standard Gibbs Free Dimerization Energies $\Delta_{dim}G°$, Absorption Maxima of the Monomer (M) and Dimer (D), and Excitonic Splittings for Dyes **1a**−**m** from UV−Vis Dilution Studies at 20 °C in Dioxane[a,b] (Standard Concentration $c°$= 1 mol L^{-1})

dye	starting material	R^1	R^2	R^3	R^4	λ_M/nm	λ_{D2}/nm	λ_{D1}/nm	$\Delta\tilde{\nu}_{D21}$/cm^{-1}	K_{dim}/L mol^{-1}	$-\Delta_{dim}G°$/kJ mol^{-1}
1a	**14e, 11b**	Dodec	Me	Dodec	H	569	492	*c*	*c*	140 000	28.8
1b	**14f, 11c**	Ethex	Me	Ethex	H	570	495	593	3 300	47 000	26.2
1c	**14a, 11a**	Hex	Me	Hex	H	568	492	597	3 600	110 000	28.2
1d	**14b, 11a**	Hex	Me	Bu	H	568	492	*c*	*c*	120 000	28.5
1e	**14c, 11a**	Hex	Me	*s*Bu	H	567	495	*c*	*c*	52 000	26.5
1f	**14d, 11a**	Hex	Me	*t*Bu	H	566	494	589	3 300	120 000	28.4
1g	**14c, 11d**	Pr	Pr	*s*Bu	H	568	497	592	3 200	18 000	23.9
1h	**14c, 11e**	*i*Pr	Pr	*s*Bu	H	570	500	602	3 400	9 700	22.4
1i	**14c, 11f**	*i*Pr	*i*Pr	*s*Bu	H	571	504	603	3 300	3 600	19.9
1j	**14g, 11g**	Ethex	Pr	Dodec	*i*Pr	562	503	604	3 300	1 900	18.4
1k	**14g, 11h**	*s*Pent	Pr	Dodec	*i*Pr	564	506	612	3 400	900	16.6
1l	**14h, 11e**	*i*Pr	Pr	Pr	*i*Pr	*d*	*d*	*d*	*d*	*d*	*d*
1m	**14i, 11i**	Bu	Me	Me	H	567	489	*c*	*c*	280 000	31.1

[a] Average from nonlinear regression analyses at four to six different wavelengths of the monomer and the dimer absorption bands. Standard deviations are about ± 0.2 kJ mol^{-1} for $\Delta_{dim}G°$. Each dye was studied at a minimum of eight different concentrations in cells of appropriate path lengths (0.01−50 mm). [b] *s*Pent = *rac*-1-methylbutyl; Ethex = *rac*-2-ethylhexyl; Dodec =1-dodecyl; *i*Pr = isopropyl; *s*Bu = *sec*-butyl. [c] Second dimer band not found. [d] Not evaluated because of limited solubility.

Scheme 2. Synthesis of Dye **2c**[a]

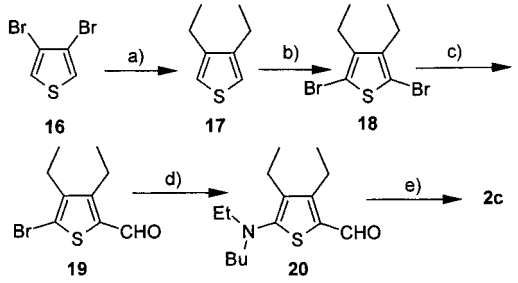

[a] Conditions: (a) EtMgBr, $NiCl_2$dppp, Et_2O, reflux under Ar, 24 h, yield 70%. (b) NBS, $CHCl_3$ and HOAc, 70 °C, 4 h, yield 90%. (c) 1. BuLi; 2. DMF, yield 78%. (d) Ethylbutylamine, toluene-4-sulfonic acid, 100 °C, 20 h. (e) **11i**, Ac_2O, 100 °C, 1 h, yield 23%.

necessary, which are collected in Scheme 2. The synthesis of dyes **3**−**8** has already been described elsewhere in the context of our previous work on the electrical and optical properties of these chromophores.[14,15,28]

Dimerization Studies for Dyes 1a−m in Dioxane. Aggregation of dyes in liquid solution is most widely studied by optical spectroscopic methods. For the dyes discussed in this paper, a significant spectral change could be observed upon variation of the concentration in the range from 10^{-6} to 10^{-1} mol/L using cells with path lengths between 0.001 and 5 cm. The UV−vis spectra in dioxane in diluted solution (10^{-6} M) can be ascribed to the monomeric dyes with the most intensive charge-transfer (CT) band occurring at longest wavelength and subsidiary vibronic maxima or shoulders at shorter wavelengths. With increasing concentration, the intensity of the CT band is reduced, and a concomitantly appearing hypsochromically shifted new band reveals the aggregation of the dyes. Over a considerable range of concentrations, well-defined isosbestic points occur in the concentration series of absorptivity curves (Figure 1) and clearly indicate the presence of equilibria between two species, i.e., monomeric (M) and dimeric (D) dyes. This allows us to formulate a simple dimerization model according to

$$K_{dim} = \frac{c_D}{c_M^{\,2}} = \frac{1-\alpha}{2\alpha^2 c_{0M}} \qquad (1)$$

where K_{dim} denotes the dimerization constant for $2M \leftrightarrows D$, c_M and c_D are the concentrations of monomer and dimer, c_{0M} is

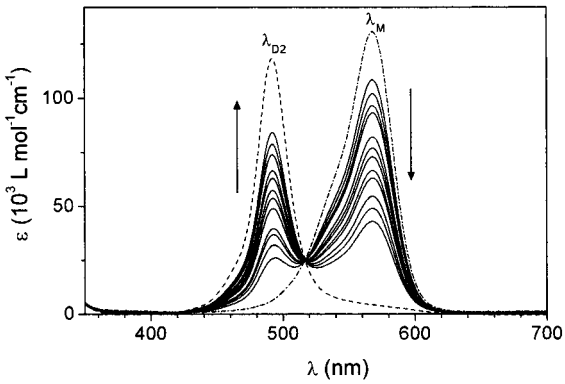

Figure 1. Concentration-dependent optical absorption spectra of dye **1d** in dioxane. The arrows indicate the decrease of the intensity of the monomer band and the appearance of a dimer band with increasing concentration from 1.0×10^{-6} to 3.0×10^{-5} M. The spectra of the monomer (−·−) and the dimer (- - -) were calculated from the data at two different concentrations and the binding constant according to eq 3. Almost identical spectral changes were observed for all dyes **1a**−**m** (see Supporting Information).

the initial (monomeric) dye concentration, and α ($=c_M/c_{0M}$) is the fraction of the monomeric dye in solution. The average (apparent) molar absorptivity ϵ of the dye in solution may be expressed in the form

$$\epsilon = \epsilon_M\alpha + (1-\alpha)\epsilon_D \qquad (2)$$

where ϵ_M and ϵ_D are the molar absorptivities of a free and the dimer-bound monomeric unit, respectively. Combining eqs 1 and 2, we obtain eq 3:

$$\epsilon = \frac{\sqrt{8K_{dim}c_{0M}+1}-1}{4K_{dim}c_{0M}}(\epsilon_M - \epsilon_D) + \epsilon_D \qquad (3)$$

Nonlinear regression analysis of the apparent molar absorptivity of the dye as a function of dye concentration at certain wavelengths based on eq 3 yields the dimerization constants K_{dim} and allows calculation of the monomer and dimer spectra. The dimerization constants and the related Gibbs dimerization energies,

$$\Delta_{dim}G° = -RT\ln K_{dim} \qquad (4)$$

for **1a**−**m** are collected in Table 1.

Table 2. Absorption Maxima λ, Dimerization Constants K_{dim}, and Standard Gibbs Free Dimerization Energies $\Delta_{dim}G^\circ$ for Dye **1a** from UV−Vis Dilution Studies at 20 °C in Various Solvents[a] (Standard Concentration $c^\circ = 1$ mol L^{-1})

solvent	ϵ_r	λ_M/ nm	λ_{D1}/ nm	λ_{D2}/ nm	$\Delta\tilde{\nu}_{D21}$/ cm^{-1}	K_{dim}/ L mol^{-1}	$-\Delta_{dim}G^\circ$/ kJ mol^{-1}
CCl_4	2.24	593	506	*b*	*b*	2 100 000	41.1
dioxane	2.22	569	492	*b*	*b*	140 000	28.8
benzene	2.27	582	505	604	3 200	72 000	27.2
TCE[c]	3.39	581	501	602	3 300	18 000	23.9
$CHCl_3$	4.81	558	489	558	2 500	520[d]	15.2
BuAc[c]	5.07	555	491	554	2 300	1 000	16.9
THF	7.52	551	493	550	2 100	65	10.2
DCE[c]	10.42	548	492	561	2 500	12	6.1

[a] Average from nonlinear regression analyses at four to six different wavelengths of the monomer and the dimer absorption band. [b] Second dimer band not found. [c] TCE = trichloroethylene; BuAc = butyl acetate; DCE = dichloroethane. [d] The same value was obtained in an NMR dilution experiment in $CDCl_3$ based on the change of ^{1}H chemical shifts.

The values of K_{dim} and $\Delta_{dim}G^\circ$ are apparently influenced by the introduction of sterically demanding alkyl groups. In general, only a small influence on the binding energy is exerted by substituents R^1 and R^3 that are attached at the peripheral edges of the dyes (**1a**−**f**,**m**). On the other hand, for the more central substituent R^2 at the pyridone acceptor heterocycle, the K_{dim} value is reduced by about 1 order of magnitude with a simple *n*-propyl substituent in place of methyl (**1g**,**h**), and a further factor of 2 was possible with the sterically more demanding isopropyl group (**1i**). Another quite efficient way to reduce the propensity for dimerization was the introduction of isopropyl substituents at the 2,6 positions of the pyridine donor heterocycle (**1j**−**l**). Upon combined application of these "high impact" substituents R^2 and R^4, a dimerization constant of 900 M^{-1} was observed for **1k**, which is 2 orders of magnitude lower than the value for **1a**, corresponding to half of the value of the Gibbs dimerization energy.

Solvent-Dependent Dimerization Studies of Dye 1a. Solvent polarity may be expressed by physical properties such as the relative permittivity ϵ_r, the dipole moment μ_g, and the refractive index *n* or by empirically derived polarity scales such as the ones of Dimroth and Reichardt ($E_T(30)$) or Kamlet and Taft (π^*).[29] Very often these scales are used to correlate energy properties based on linear free energy relationships. The dimerization of the merocyanine dyes is characterized by a free dimerization energy which should be highly dependent on the polarity of the solvent if dipolar interactions make the main contribution. Therefore, the dimerization constants were evaluated for **1a** in a number of solvents with different polarities (Table 2 and Figure 2; for spectra refer to the Supporting Information).

The occurrence of dimer bands and isobestic points in the concentration-dependent spectra indicates the formation of dimers in all solvents but within quite different concentration ranges. As expected, the dimerization process turns out to be very sensitive to the polarity of the solvent that is expressed in terms of the relative permittivity, ϵ_r, in Table 2. In the most polar solvent, dichloroethane (DCE), a dimerization constant of 12 M^{-1} is obtained, which is 6 orders of magnitude lower than the value of 2×10^7 M^{-1} in the least polar solvent, tetrachloromethane. Accordingly, significantly higher concentrations than in tetrachloromethane are necessary to observe aggregate formation in polar environments such as DCE.

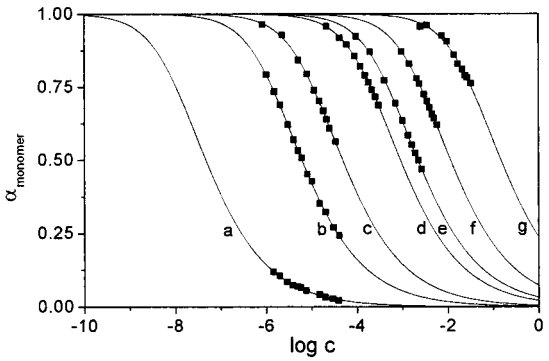

Figure 2. Fraction of monomer ($\alpha_{monomer}$) calculated from UV−vis data at certain wavelengths (■) in various solvents and results of the nonlinear regression analysis (−) based on eq 3 for dye **1a**: (a) in tetrachloromethane at 594 nm, (b) in dioxane at 505 nm, (c) in trichloroethylene at 505 nm, (d) in chloroform at 500 nm, (e) in butyl acetate at 500 nm, (f) in tetrahydrofurane at 495 nm, (g) in dichloroethane at 505 nm; c = concentration in moles per liter.

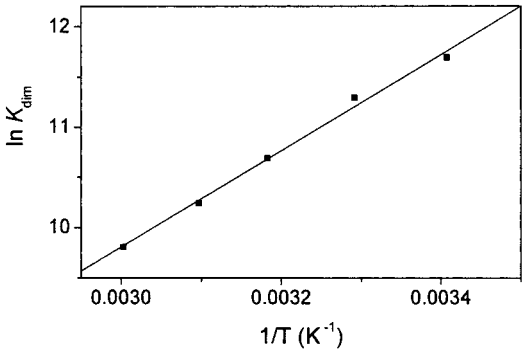

Figure 3. Van't Hoff plot for the temperature dependence of the dimerization constant of **1a** in dioxane solution.

Temperature-Dependent Dimerization Studies for Dye 1a in Dioxane. The enthalpy and entropy contributions to the Gibbs dimerization energy of dye **1a** were obtained by means of a van't Hoff plot according to eq 5 from temperature-dependent

$$-RT \ln K_{dim} = \Delta_{dim}H^\circ - T\Delta_{dim}S^\circ \qquad (5)$$

UV−vis experiments, where the dimerization constants K_{dim} were determined at five different temperatures by nonlinear regression analysis as outlined above.The plot of ln K_{dim} versus T^{-1} shows a linear relationship with correlation coefficient $r = 0.997$ (Figure 3). The standard dimerization enthalpy and entropy were determined to be $\Delta_{dim}H^\circ = -39.8 \pm 1.7$ kJ mol^{-1} and $\Delta_{dim}S^\circ = -37.9 \pm 5.5$ J mol^{-1} K^{-1}, indicating an enthalpy-driven dimerization process.

Dimerization Studies for Dyes 2−8 in Dioxane. The dimerization model was equally applicable to describe the concentration dependence of the UV−vis spectra of dyes **2**−**8**. Two examples are shown in Figures 4 and 5 for the dyes **5b** and **7**, which again exhibit hypsochromically shifted dimer bands and well-defined isosbestic points. A similar behavior was found for all other dyes of this study (Figure 6), the spectra of which are displayed in the Supporting Information. In all cases, dimerization constants and Gibbs dimerization energies could be derived from eqs 1−4. From the values given in Table 3, we conclude that, in addition to the already mentioned sterical

(29) Reichardt, C., Ed. *Solvents and Solvent Effects in Organic Chemistry 2*; VCH: Weinheim, 1990.

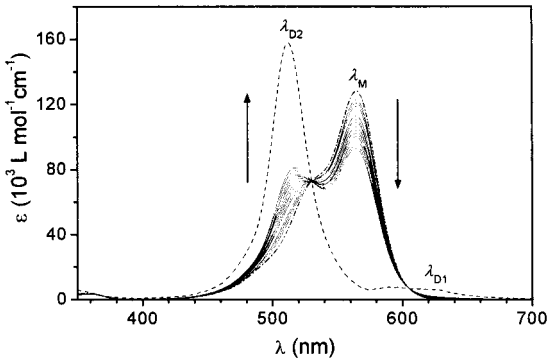

Figure 4. Concentration-dependent optical absorption spectra of dye **5b** in dioxane. The arrows indicate changes of the monomer and the dimer bands upon increasing concentration from 2.0×10^{-5} to 2.7×10^{-4} M. The spectra of the monomer (—•—, $\lambda_M = 565$ nm) and the dimer (- - -, $\lambda_{D1} = 512$ nm, $\lambda_{D2} = 590$ nm) were calculated as described in Figure 1.

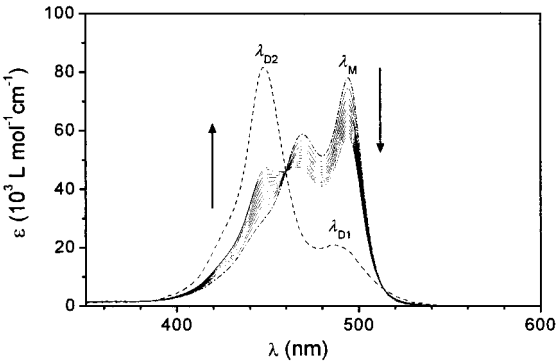

Figure 5. Concentration-dependent optical absorption spectra of dye **7** in dioxane. The arrows indicate changes of the monomer and the dimer bands upon increasing concentration from 1.1×10^{-4} to 2.6×10^{-3} M. The spectra of the monomer (-•-, $\lambda_M = 494$ nm) and the dimer (- - -, $\lambda_{D1} = 448$ nm, $\lambda_{D2} = 487$ nm) were calculated as described in Figure 1.

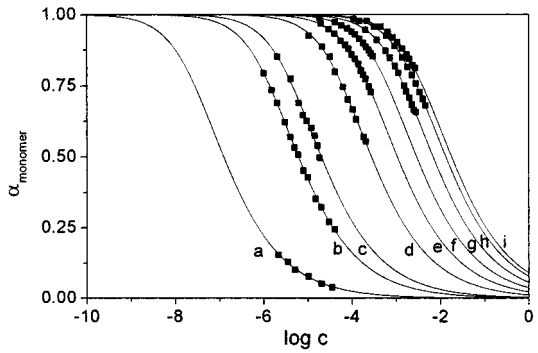

Figure 6. Fraction of monomeric dyes **2**—**8** calculated from experimental data at certain wavelengths (■) and the calculated lines (—) based on the dimerization constants given in Table 3: (a) **8** at 690 nm, (b) **1a** at 505 nm, (c) **3** at 590 nm, (d) **5c** at 635 nm, (e) **5b** at 510 nm, (f) **5a** at 430 nm, (g) **6** at 475 nm, (h) **2a** at 505 nm, and (i) **7** at 455 nm; c = concentration in moles per liter.

factors, a significant influence can be attributed to the dipolar nature of the dyes and the length of the π-conjugated system. The progressive increase of binding constants from **6** to **1c** and to **8** is evidently due to the increase of the dipole moment caused by more and more electron-withdrawing acceptor heterocycles. Another interesting series of dyes is given with **5a**—**c** that also exhibit a gradual increase of the binding constant concomitantly with the extension of the conjugated system. In addition to increased dipole interactions within this series, the enlargement

Table 3. Ground- and Excited-State Dipole Moments μ_g and μ_a from EOAM and Absorption Maxima λ, Dimerization Constants K_{dim}, and Standard Gibbs Free Dimerization Energies $\Delta_{dim}G°$ from UV—Vis for Dyes **2**—**8** in Dioxane at 20 °C (Standard Concentration $c° = 1$ mol L^{-1})

dye	$\mu_g/10^{-30}$ C m	$\mu_a/10^{-30}$ C m	λ_M/ nm	λ_{D1}/ nm	λ_{D2}/ nm	$\Delta\tilde{\nu}_{D21}$/ cm^{-1}	K_{dim}[a]/ L mol^{-1}	$-\Delta_{dim}G°$/ kJ mol^{-1}
1m	57	42	567	489	*b*	*b*	280 000	31.1
2a	47	53	535	503	551	1 700	75	10.5
3	52	45	633	559	*b*	*b*	47 000	26.2
4a	43	49	520	*c*	*c*	*c*	<5	<4[c]
5a	44	47	462	429	493	3 000	460	15.2
5b	47	56	565	512	590	2 600	1 100	17.4
5c	50	83	660	590	661	1 800	3 700	20.4
6	40	31	515	476	*b*	*b*	110	11.6
7	50	45	494	448	487	1 800	160	12.6
8	64	48	671	554	*b*	*b*	8 000 000	39

[a] Average from nonlinear regression analyses at four to six different wavelengths of the monomer and the dimer absorption bands. [b] Second dimer band not found. [c] For dyes **4a**,**b**, no aggregation could be observed in the solvents dioxane and tetrachloromethane up to a concentration of 2×10^{-2} mol L^{-1}.

of the interacting molecular surfaces (related to van der Waals interactions) may also contribute to this effect. Remarkably, the dyes **2a**, **5b** and **4a**,**b** have the same acceptor unit and similar dipole moments but show significantly different interaction energies. It seems reasonable to suspect that the bent shape of **2a** makes the antiparallel alignment of two dye molecules less efficient compared to that in the linear dye **5b** (see also the crystal structure of **2c**). The fact that no aggregation could be observed for dyes **4a**,**b** within the concentration range accessible with our instrumentation can be rationalized by the high steric demand of the 3,3′-dimethylmethylene unit of the electron-donating indoline heterocycle.

Structural Characterization in Solution by 2D NMR Spectroscopy. In a closely packed dimer, spatial proximities between nearby protons of the two individual molecules should lead to faster spin relaxation rates, owing to dipolar through-space couplings which can be studied by nuclear Overhauser effect (NOE) spectroscopy. Since the signal intensity of the NOE becomes very low in the intermediate mass range, in our case (the masses of the dimers are around 1000 g/mol) the rotating-frame Overhauser enhancement spectroscopy (ROESY) technique was applied. For these experiments, high concentrations of predominantly dimerized molecules (which require high binding constants) as well as protons with distinct chemical shifts are desirable, which suggested dye **1b** as a good candidate. First, full assignment of the protons and carbons of the monomeric dye **1b** was accomplished by two-dimensional homonuclear HMQC and HMBC measurements in THF-d_8, where the dye has a very low binding constant and insignificant amounts of dimers are present even at high concentration. The through-space connectivities were then determined by ROESY in dioxane-d_8 at a concentration of 5 mM, where the dimerization is almost complete (~96%, calculated from $K_{dim} = 4.7 \times 10^4$ M^{-1}) and in $CDCl_3$, where monomeric dyes prevail due to the lower dimerization constant. In $CDCl_3$, no intermolecular cross coupling could be found, and all ROE signals could be assigned to intramolecular through-space couplings. In contrast, two new cross-peaks appeared in the ROE spectrum in dioxane, i.e., H_4—H_6 and H_3—H_7, respectively (Figure 7). For those two pairs of protons, the intermolecular distances in a centrosymmetric dimer according to Figure 8 are 2.6 and 2.9 Å (based

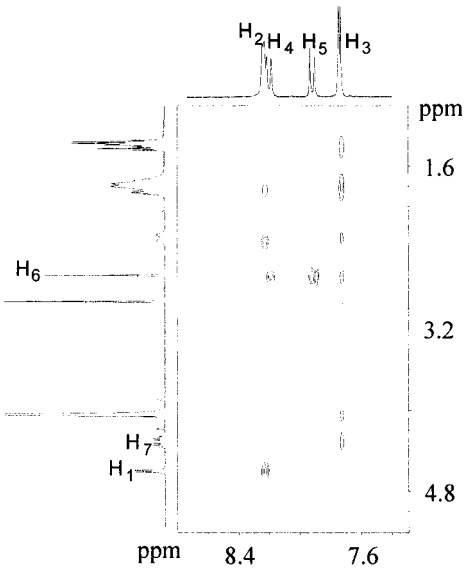

Figure 7. Selected area of the ROESY NMR spectrum for a 5 mM solution of dye **1b** in dioxane-d_8 at 300 K.

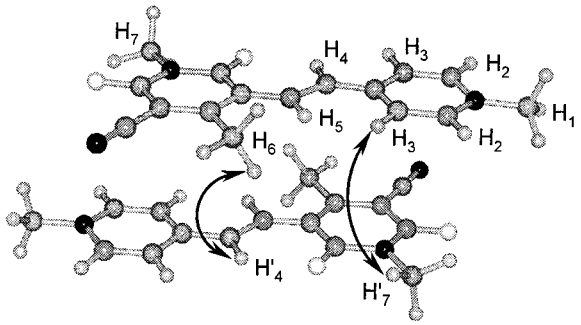

Figure 8. Structural model for the dimeric unit $(\mathbf{1b})_2$ in solution based on the NMR studies and AM1 geometry-optimized molecules. The arrows indicate spatial proximities as evidenced by ROESY cross coupling peaks (only half of which are shown in Figure 7). All alkyl substituents were replaced by methyl for simplicity.

on AM1-optimized molecules[30]), which are well within the range of ROESY experiments, whereas the intramolecular distances between these protons within the same molecule (5.0 and 6.5 Å) are far beyond the sensitivity of this technique. These results strongly indicate the existence of centrosymmetric dimers with a structure similar to the one illustrated in Figure 8.

Structural Characterization in the Solid State by X-ray Crystallography. Further evidence for the formation of dimeric aggregates is provided by structure determination of dyes in the solid state by X-ray crystallography. Although it is often difficult to grow single crystals of sterically crowded and/or highly dipolar dyes, crystals of dyes **1l** and **2c** suitable for crystallographic structure analysis could be obtained by slow crystallization from a hexane/ethanol solution at low temperature. The ORTEP view of the molecular structure of **1l** is shown in Figure 9. Despite of the considerable number of bulky substituents, an almost undisturbed π-conjugated system is observed which is nearly coplanar (twisting angle of 11° between the mean planes of the pyridone and the pyridine rings) and reveals significant bond length equilibration within the conjugated path. Thus, with a bond length of 1.35 Å for the

(30) CAChe for Windows, version 3.2; Oxford Molecular Group, Inc., USA, 1999; see http://www.oxmol.com

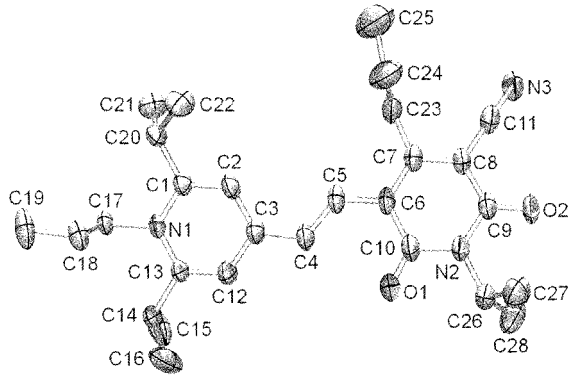

Figure 9. ORTEP drawing of the structure of **1l** in the crystal with atomic numbering and selected bond distances. Hydrogen atoms were omitted for clarity.

Table 4. Selected Bond Distances for **1l** in the Crystal[a]

atom 1	atom 2	bond length (Å)	atom 1	atom 2	bond length (Å)
C13	N1	1.383(3)	C6	C7	1.411(4)
C12	C13	1.357(4)	C7	C8	1.383(4)
C1	N1	1.387(3)	C8	C9	1.431(4)
C1	C2	1.368(4)	C6	C10	1.450(4)
C2	C3	1.402(4)	O2	C9	1.234(3)
C3	C12	1.407(4)	N2	C9	1.390(4)
C3	C4	1.435(4)	N2	C10	1.416(4)
C4	C5	1.354(4)	O1	C10	1.236(4)
C5	C6	1.441(4)			

[a] Esd's in parentheses refer to the last digit.

Chart 2

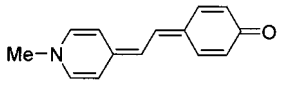

21

central C4—C5 bond, almost the distance of a C=C double bond is maintained (standard single-bond and double-bond values 1.46 and 1.34 Å, respectively),[31] indicating a significant displacement of electron density (or charge transfer) from the donor to the acceptor part, corresponding to a large contribution of the zwitterionic resonance structure in this merocyanine dye. This conclusion is also supported by the other bond lengths given in Table 4. For comparison, the well-known Brooker dye 4-{2-[1-methyl-4-(1*H*)-pyridylidene]ethylidene}cyclohexa-2,5-dien-1-one (**21**, Chart 2), which has a similar conjugated backbone and a length of the central bond of 1.35 Å in the solid state, is considered as the prototype of a zwitterionic merocyanine dye, with a estimated degree of 81.8% for the zwitterionic form.[32] Thezwitterionic character of the structure is also corroborated by the negative solvatochromism of dye **1a**,[33] i.e., red shift of the monomer absorption band with decreasing solvent polarity (Table 2).

The observed arrangement of the dyes in the crystal is fully consistent with the solution 2D NMR experiments. As can be seen from Figure 10, even in the presence of three bulky isopropyl substituents, a centrosymmetric unit of two dyes is formed which are now, however, considerably slipped apart to

(31) Sutton, L. E. In *Tables of Interatomic Distances and Configuration in Molecules and Ions, Special Publication No. 18*; Mitchell, A. D., Somerfield, A. E., Cross, L. C., Eds.; The Chemical Society: London, 1965.
(32) De Ridder, D. J. A.; Heijdenrijk, D.; Schenk, H.; Dommisse, R. A.; Lemiere, G. L.; Lepoivre, J. A.; Alderweireldt, F. A. *Acta Crystallogr.* **1990**, *C46*, 2197−2199.
(33) For the solvatochromic properties of dyes of type **21**, see ref 39.

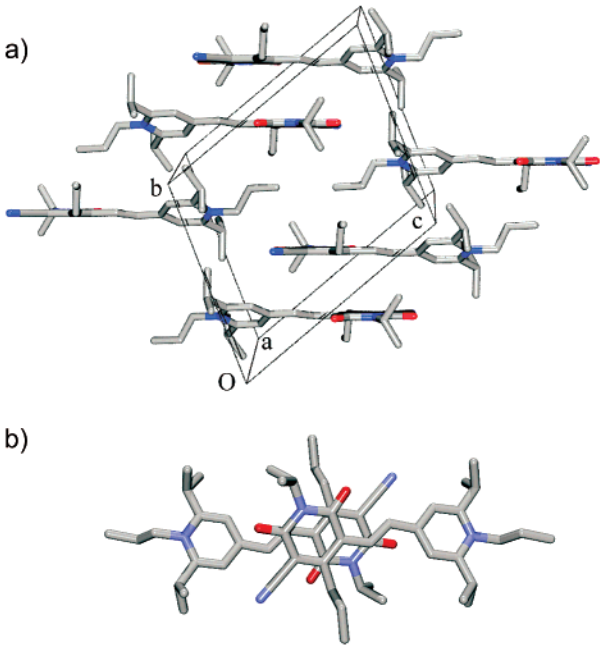

Figure 10. Molecular packing of **1l** in the crystal. (a) View at the *bc* plane showing the packing of the dyes in columns with a close and a more distant neighbor. (b) Top view of the dimeric unit.

accommodate the bulky side chains. Owing to this displacement, the two neighboring π-conjugated systems may approach close to the smallest possible van der Waals distance between two π-systems, i.e., 3.5 Å. This face-to-face arrangement leads to a densely packed dimer that optimizes not only the dispersion interactions but also the electrostatic energy because of the antiparallel orientation of the highly dipolar dye molecules. The isopropyl groups of the pyridone rings are located over the methine chain of the neighboring dye, and the two isopropyl groups at the pyridine donor heterocycles find enough space as a result of the displacement. Compared to the geometry of the sterically less critical dimer $(\mathbf{1b})_2$ in solution, we note that the two (negatively charged) pyridone acceptor groups lay on top of each other in the dimeric unit $(\mathbf{1l})_2$, which should be energetically less favorable and may account for the reduced interaction energy of dyes **1l** in solution.

A second interesting structural motif, the packing of the dimeric units in the crystal, is revealed in Figure 10a. Thus, the dimers pack in an antiparallel fashion along the *c*-axis, which further minimizes the electrostatic energy despite the now considerably larger distance between the π-systems (~5.6 Å). The reasons for the larger distance may be attributed to the alkyl chains, which have to point away from the contact surface of the densely packed dimeric unit to allow for the close contact of 3.5 Å. As a consequence, the distance to the second neighbor has to be increased. Such structural features might also explain why we did not find any evidence for more extended aggregates than dimers in the concentration-dependent UV−vis experiments for the whole series of merocyanine dyes.

Structural and packing features similar to those for **1l** are observed for the less polar and sterically less crowded merocyanine dye **2c**. As shown in Figures 11 and 12, **2c** exhibits a coplanar π-conjugated system with a twisting angle of only 7° between the mean planes of the thiophene and the pyridone rings, and the observed bond length alternations again indicate a high contribution of a zwitterionic resonance structure (Table 5). The central C4−C5 bond length of the methine bridge is now 1.37 Å, which is larger than in **1l** but still shorter than the 1.42 Å of the C5−C6 bond. Other features which support the high conjugation between the donor and the acceptor parts are the short N1−C1 bond length of 1.34 Å, the sp^2 hybridization of the dimethylamino nitrogen (dihedral angles of 19.4° for C19−N1−C1−C2 and 9.4° for C17− N1−C1−C2), and the quinonoid geometry of the thiophene ring, which exhibits longer

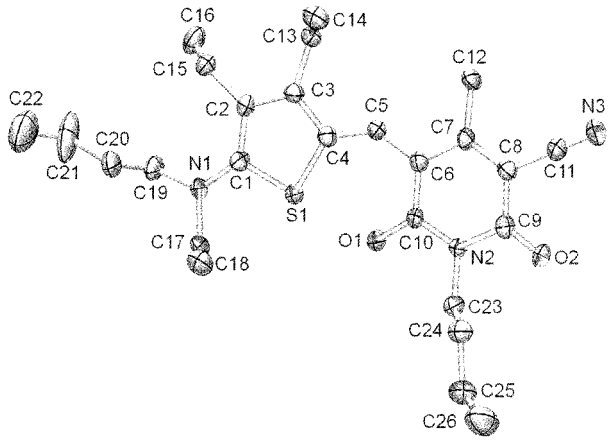

Figure 11. ORTEP drawing of the structure of **2c** in the crystal with atomic numbering and selected bond distances. Hydrogen atoms were omitted for clarity.

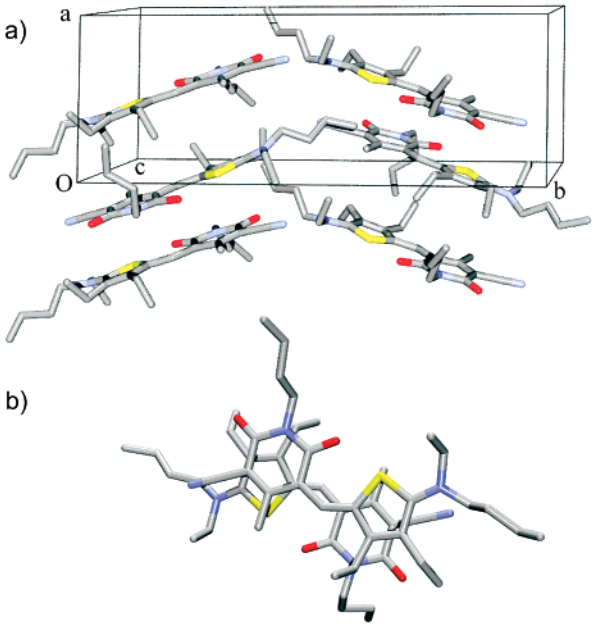

Figure 12. Molecular packing of **2c** in the crystal. (a) View at the *ab* plane showing packing of the dyes in columns with a close and a more distant neighbor. (b) Top view of the dimeric unit.

Table 5. Selected Bond Lengths for **2c** in the Crystal[a]

atom 1	atom 2	bond length (Å)	atom 1	atom 2	bond length (Å)
C1	N1	1.340(5)	C6	C7	1.416(5)
C1	S1	1.728(4)	C7	C8	1.368(6)
C1	C2	1.434(5)	C8	C9	1.447(5)
C2	C3	1.371(5)	C6	C10	1.448(5)
C3	C4	1.447(5)	O2	C9	1.226(5)
S1	C4	1.749(4)	N2	C9	1.395(5)
C4	C5	1.370(6)	N2	C10	1.400(5)
C5	C6	1.423(5)	O1	C10	1.229(4)

[a] Esd's in parentheses refer to the last digit.

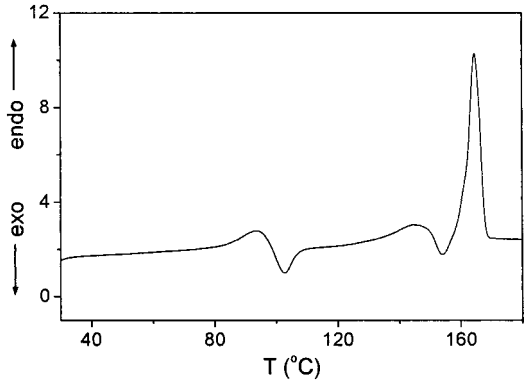

Figure 13. DSC trace of dye **1c** showing the heat flows within the first heating cycle at 10 K min^{-1}. The heat of the melting transition at 165 °C amounts 39 J g^{-1}.

carbon−carbon distances for the $C_\alpha-C_\beta$ formal single bonds and a shorter distance for the $C_\beta-C_\beta$ formal double bond, i.e., 1.43, 1.37, and 1.45 Å for C1−C2, C2−C3, and C3−C4, respectively.

In the unit cell of dye **2c** (Figure 12), again centrosymmetric dimers of **2c** are packed face-to-face, as observed for dye **1l**. Owing to the lower sterical congestion compared to **1l**, the two π-systems may now approach at a distance as close as 3.40 Å, and the thiophene donor and pyridone acceptor heterocycles are positioned on top of each other, which supposedly is the most ideal packing, which was also found in solution NMR studies for the dimer of dye **1b**. On the other hand, the top view of the dimer (Figure 12b) also reveals some constraints for these bent-shaped monomethine dyes that cannot perfectly superimpose the whole π-conjugated chain on top of each other, in contrast to their linear dimethine counterparts. This restriction probably accounts for the lower binding constants of **2a**−**c** in solution. In the dimeric unit of the crystal, all but one alkyl substituent point away from the center of the dimer. As for **1l**, this arrangement allows for a close contact of the two π-systems within the dimer at a distance of only 3.40 Å but demands a larger distance (4.60 Å) to the next neighbor. While this distance is out of the range of $\pi-\pi$ interactions, the antiparallel arrangement again suggests electrostatic forces to be of primary importance for the packing of the dyes in the solid state.

Finally, a remarkable propensity of these merocyanine dyes to form amorphous solids or microcrystalline powders was observed. This was already mentioned above in the context of the difficulties experienced for obtaining suitable crystals for single-crystal X-ray diffraction. Differential scanning calorimetric (DSC) studies for several of the dyes in this study showed a complex phase behavior, a typical example (**1c**) being displayed in Figure 13. Two morphological transitions occur at about 100 and 150 °C before the compound melts at 160 °C. For a significant number of merocyanine dyes, cooling with rates of 10 K min^{-1} does not lead to recrystallization but to formation of amorphous solids. The propensity for glass formation was utilized in our prior work on organic photorefractive materials based on merocyanine dyes **2** and **4** with indoline and aminothiophene donor groups.[28,34] This peculiar

(34) (a) Würthner, F.; Yao, S.; Schilling, J.; Wortmann, R.; Redi-Abshiro, M.; Mecher, E.; Gallego-Gomez, F.; Meerholz, K. *J. Am. Chem. Soc.* **2001**, *123*, 2810−2814. (b) Mecher, E.; Gallego-Gomez, F.; Bräuchle, C.; Meerholz, K.; Wortmann, R.; Yao, S.; Sautter, A.; Würthner, F. *Proc. SPIE* **2000**, *4104*, 118−129.

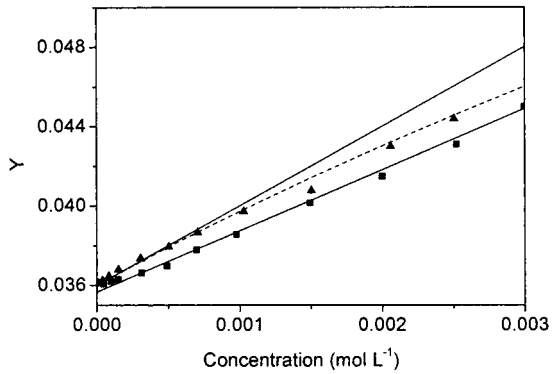

Figure 14. Dipole moment measurements of dyes **2b** (▲) and **4b** (■) in dioxane with $Y = (\epsilon_r - 1)/(\epsilon_r + 2) - (n^2 - 1)/(n^2 + 2)$. The solid lines show the calculations according to eq 6 under the assumption of ideal non-interacting dyes **2b** ($\mu_{gM} = 47 \times 10^{-30}$ Cm) and **4b** ($\mu_{gM} = 43 \times 10^{-30}$ Cm). The dashed line shows the calculation according to eq 7, where the dimerization to a centrosymmetric dimer ($K_{dim} = 30\ M^{-1}$) was considered.

behavior may tentatively be attributed to the high interaction energies in the dimeric units which do not easily slip to another arrangement to form a densely packed crystal. At higher temperature, the mobility of the dyes increases due to the large negative entropy associated with dimerization (see above), and a more ideal crystal packing is achieved, as indicated by the morphological transitions in Figure 13.

Dipole Moment Measurements. The centrosymmetric arrangement of the dyes in the crystalline states implies a zero dipole moment of the dimers in contrast to the large dipole moments of the monomeric dyes. As a consequence, the apparent dipole moment of the dye solution should also change with increasing concentration due to aggregation. This could be quantitatively verified by dipole moment measurements for four selected dyes with varying dimerization constants. In contrast to the EOAM method discussed below, the most common method for dipole moment elucidation is based on dielectric and refractive index measurements according to Debye's theory. In the simplest analysis according to Guggenheim and Smith, the changes in the dielectric constant and the refractive index of solutions of a polar solute (i.e., the dye) in a nonpolar solvent are measured within a condenser cell and a refractometer, respectively, and evaluated according to eq 6 by linear regression analysis.[35] In this equation, c denotes the molar

$$\frac{\epsilon_r - 1}{\epsilon_r + 2} - \frac{n^2 - 1}{n^2 + 2} = \frac{4\pi N_A \mu_g^{\,2}}{9 k_B T} c + \text{const.} \qquad (6)$$

concentration of the solute, ϵ_r the dielectric constant of the solution, n the refractive index of the solution, k_B the Boltzmann constant, N_A Avogadro's number, and μ_g the dipole moment of the solute. For nonaggregated (i.e., noninteracting) dyes, a linear relationship is typically observed if the left side of eq 6 is plotted against the concentration of the solute, and from the slope the prefactor of the right side is deduced. Such a linear behavior was indeed observed for dye **4b** (Figure 14, squares), with a correlation coefficient $r = 0.999$ and a calculated dipole moment of 43×10^{-30} Cm (=13 D) that exactly corresponds to the result obtained by EOAM (Table 3). In contrast, in the case of aggregating dyes, a concentration-dependent deviation toward

(35) (a) Guggenheim, E. A. *Trans. Faraday Soc.* **1949**, *45*, 714−720. (b) Janini, G. M.; Katrib, A. H. *J. Chem. Educ.* **1983**, *60*, 1087−1088.

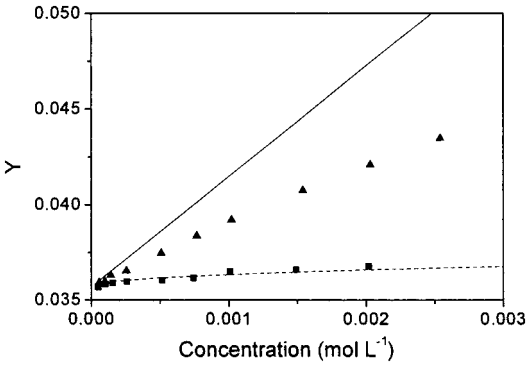

Figure 15. Dipole moment measurements of dyes **1b** (■) and **1j** (▲) in dioxane with $Y = (\epsilon_r - 1)/(\epsilon_r + 2) - (n^2 - 1)/(n^2 + 2)$. The lines show the calculations according to eqs 6 and 7 with $\mu_{gM} = 57 \times 10^{-30}$ Cm for non-interacting dyes (—) and aggregating dyes with a dimerization constant of 4.7×10^4 M^{-1} (- - -), respectively.

smaller values (i.e., saturation behavior) is observed, and smaller dipole moments are calculated by linear regression analysis. Thus, for the weakly aggregating dye **2b** (Figure 14, triangles), the dipole moment calculated according to eq 6 from the concentration-dependent increase of ϵ_r and n is only 40×10^{-30} Cm, compared to the EOAM value of 47×10^{-30} Cm. Even more significant are the deviations in the case of the strongly aggregating dyes **1b** (Figure 15, squares) and **1j** (Figure 15, triangles), where the concentration-dependent increase of ϵ_r and n afforded values $\mu_g = 17 \times 10^{-30}$ Cm for **1b** and $\mu_g = 40 \times 10^{-30}$ Cm for **1j** that fall far below the EOAM dipole moment of this chromophore ($\mu_g = 57 \times 10^{-30}$ Cm, Table 3). However, considering the dimerization constants given in Table 1, one can calculate that dyes **1b** are largely dimerized throughout the whole concentration range of the given experiment, whereas the amount of dimerization continuously increases for **1j** with increasing concentration, as suggested by the saturation behavior of the curve (Figure 15, triangles). Clearly, in such a situation, eq 6, which was derived under the assumption of noninteracting solute molecules, is not applicable. Taking into account the equilibrium of two species, a monomer with the dipole moment obtained by EOAM and a dimer with a zero dipole moment, calculations according to the suitably modified eq 7 reproduced the experimental data for the two dyes **1b** and **2b** (dashed lines in Figures 14 and 15) fairly well:

$$\overline{\mu_g^2} = \frac{1}{c_{0M}}(c_M \mu_{gM}^2 + 2c_D \mu_{gD}^2) \tag{7}$$

In this equation, $\overline{\mu_g^2}$ denotes the averaged square of the dipole moment, μ_{gM}, μ_{gD} the ground-state dipole moments, and c_M, c_D the concentrations of the monomeric (M) and the dimeric (D) species. The monomer concentration was obtained using eq 1 and the dimerization constant given in Table 1 according to

$$c_M = \frac{\sqrt{8K_{dim}c_{0M} + 1} - 1}{4K_{dim}} \tag{8}$$

The good fit results obtained with this model for dyes **1b** and **2b** further support the idea of centrosymmetric dimer formation in solution. Only for **1j** were slight deviations from this simple model observed in the fitting, which may tentatively be ascribed to the occurrence of another type of aggregate for this dye at higher concentration with a dipole moment different from zero.

Electrooptical Absorption Measurements. The dipole moments of the monomeric dyes were determined by electrooptical absorption measurement (EOAM) in dioxane.[36] An advantage of this technique is that it can be used at high dilution (typically about 10^{-5} M), where the majority of the merocyanine dyes did not show notable dimerization. In an EOAM experiment, one detects the influence of an external electric field on the optical density, $a = \epsilon c$, of the solution. The measurements are carried out for two polarizations of the incident light ($\phi = 0°$, 90°, i.e., parallel and perpendicular to the applied field) and for several wavenumbers $\tilde{\nu}$ within the absorption band. The effect of the electric field on the optical density may be described as second order in the field E by the quantity[36a]

$$L(\phi,\tilde{\nu}) = \frac{a^E(\phi,\tilde{\nu}) - a(\tilde{\nu})}{a(\tilde{\nu})}\frac{1}{E^2} \tag{9}$$

where $a^E = \epsilon^E c^E$ is the optical density of the solution in the presence of the field E. Usually the dye concentration is not field dependent, so that $c^E = c$. The field induces then only a change of the molar decadic absorption coefficient ϵ. The two main contributions to this change are due to the electrodichroism caused by partial alignment of the dipolar dye molecules and to the band shift caused by charge redistribution in the externally applied field. These effects can be quantitatively determined by a numerical band shape analysis[36] and yields among other information the ground state (g) and excited state (a) dipole moments, μ_g and μ_a, of the dyes. The values are summarized in Table 3.

In case of chemical equilibria, there may be also an electric field effect on the concentration, as has been shown by Liptay et al.[37] This effect may be expected to be particularly strong if the reacting species strongly differ in their dipole moments, as is the case here with the monomeric and dimeric merocyanine dyes. The field dependence of the concentration is an isotropic effect that—to second order in the field—does not depend on the polarization of the incident light. Taking into account field-dependent concentrations, eq 9 becomes

$$L(\phi,\tilde{\nu}) = \frac{\epsilon^E(\phi,\tilde{\nu}) - \epsilon(\tilde{\nu})}{\epsilon(\tilde{\nu})}\frac{1}{E^2} + \frac{1}{2c}\frac{\partial^2 c}{\partial E^2} \tag{10}$$

For more than one absorbing species, eq 10 has to be generalized by summation over all absorbing reactants. For the dimerization equilibrium eq 1, the field dependence of the concentrations may be expressed by the field dependence of the dimerization constant that is given by

$$K_{dim}{}^E = K_{dim}\exp(-\Delta_{dim}G^E/RT) \tag{11}$$

where $K_{dim}{}^E$ is the dimerization constant within the field and $\Delta_{dim}G^E$ the field-dependent contribution to the Gibbs enthalpy

(36) (a) Liptay, W. In *Excited States, Vol. 1. Dipole Moments and Polarizabilities of Molecules in Excited Electronic States*; Lim, E. C., Ed.; Academic Press: New York, 1974; pp 129—229. (b) Wortmann, R.; Elich, K.; Lebus, S.; Liptay, W.; Borowicz, P.; Grabowska, A. *J. Phys. Chem.* **1992**, *96*, 9724—9730. (c) Bublitz, G. U.; Boxer, S. G. *Annu. Rev. Phys. Chem.* **1997**, *48*, 213—242.

(37) Liptay, W.; Rehm, T.; Wehning, D.; Schanne, L.; Baumann, W.; Lang, W. *Z. Naturforsch. A* **1982**, *37*, 1427—1448.

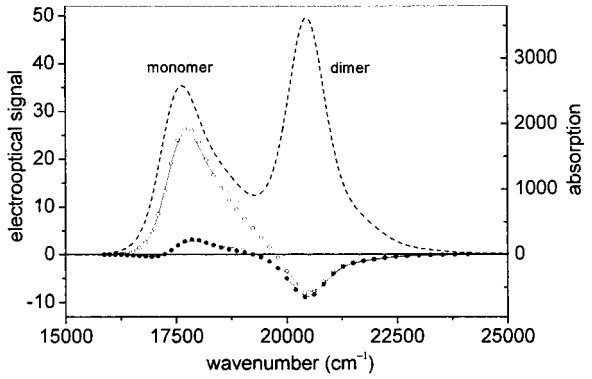

Figure 16. Optical absorption ($\epsilon/\tilde{\nu}$)/cm^3 mol^{-1} (– – –, right scale) and electrooptical absorption signal ($L\epsilon/\tilde{\nu}$)/10^{-10} cm^3 V^{-2} mol^{-1} of chromophore **1m** in dioxane at a concentration of 5.9×10^{-6} mol L^{-1}, $T = 298$ K. Electrooptical data points are shown for parallel (○: $\varphi = 0°$) and perpendicular polarization (●: $\varphi = 90°$) of the incident light relative to applied electric field and multilinear regression curves in the regions of monomer and dimer bands.

of the reaction. The latter quantity may be estimated according to the theory by Liptay,[37] which yields after minor modifications and assuming a vanishing dipole moment of the dimer the following expression:

$$\Delta_{\mathrm{dim}}G^E = \frac{N_\mathrm{A}}{3k_\mathrm{B}T}L^2{\mu_\mathrm{g}}^2E^2 \qquad (12)$$

where L is a Lorentz local field factor. With eqs 1 and 8, it follows for the relative field dependencies of the concentrations in the monomer and dimer band to second order:

$$L_{c_\mathrm{M}} = \frac{1}{2c_\mathrm{M}}\frac{\partial^2 {c_\mathrm{M}}^E}{\partial E^2} = \frac{c_{0\mathrm{M}} - c_\mathrm{M}}{2(2c_{0\mathrm{M}} - c_\mathrm{M})}\frac{L^2{\mu_\mathrm{gM}}^2}{3{k_\mathrm{B}}^2T^2} \qquad (13)$$

$$L_{c_\mathrm{D}} = \frac{1}{2c_\mathrm{D}}\frac{\partial^2 {c_\mathrm{D}}^E}{\partial E^2} = -\frac{c_\mathrm{M}}{2(2c_{0\mathrm{M}} - c_\mathrm{M})}\frac{L^2{\mu_\mathrm{gM}}^2}{3{k_\mathrm{B}}^2T^2} \qquad (14)$$

where L_{c_M} and L_{c_D} have been introduced as abbreviations and c_M has been defined in eq 8. Equations 13 and 14 show that the external field increases the monomer concentration at the expense of the dimer concentration.

For the strongly polar dye **1m**, we indeed were able to observe such an electric field effect on the concentration. This dye dimerizes sufficiently even at the low concentrations of the EOAM experiment, and its UV−vis absorption spectrum clearly shows monomer and dimer maxima corresponding to a dimerization constant of $K_\mathrm{dim} = 280\,000$ M^{-1}. The electrooptical spectrum of **1m** taken at a concentration of $c_{0\mathrm{M}} = 5.9 \times 10^{-6}$ M and a temperature of $T = 298$ K is displayed in Figure 16. Large electrooptical signals are observed in the region of the monomeric band due to the large monomer dipole moment and the corresponding electrodichroic effect. In contrast, the signals are much lower in the region of the dimer absorption band due to its small or vanishing dipole moment. Closer inspection shows that the electrooptical signals are even negative within the dimer band, in accordance with an expected negative contribution from the concentration term (cf. eqs 10 and 14). Polarization-dependent EOAM experiments allow us to separate the two terms on the right-hand side of eq 10 within the monomer and dimer band. The results are $L_{c_\mathrm{M}} = 3800 \times 10^{-20}$ m^2 V^{-2} and $L_{c_\mathrm{D}} = -2300 \times 10^{-20}$ m^2 V^{-2}. Applying eqs 13 and 14 with a dipole moment of $\mu_\mathrm{gM} = 57 \times 10^{-30}$ C m and Lorentz local field factors of $L = 1.4$, we obtain $L_{c_\mathrm{M}} = 2300 \times 10^{-20}$ m^2 V^{-2} and $L_{c_\mathrm{D}} = -1700 \times 10^{-20}$ m^2 V^{-2}, which are in reasonable agreement with the experimental values.

Discussion

The results obtained for merocyanine dyes **1**−**8** provide a fairly complete and general picture of the dimerization of these dyes in solution as well as their packing in the solid state. In the following discussion, we interpret the intermolecular forces that direct the dimerization process and discuss the solvent dependence as well as the changes of the absorption spectra upon dimerization. In the last section we will discuss the implications of the results to nonlinear optical and photorefractive applications that rely on the orientation of dipolar dyes in an external electric field.

We begin the discussion from a structural point of view and with a comment on why such a common aggregation process has been rarely observed in solution before, despite the vivid interest in merocyanines for decades, in both the chemistry and the applications of these dyes in new technologies. One reason is probably the typically low solubility of simple merocyanines that bear only small substituents such as hydrogen or methyl. Such dyes form very stable crystal lattices and accordingly dissolve only in "good" solvents that provide strong dipolar and dispersion interactions with the dye molecules. However, in such solvents no aggregation takes place within the typical concentration range of optical spectroscopy.

On the other hand, centrosymmetric arrangements of dyes including merocyanines have been found in a number of crystallographic studies on organic NLO chromophores with large ground-state dipole moments.[32,38] It is indeed believed that the centrosymmetric packing of dipolar dyes is the most common structural motif in the solid state and does account for the failure of most organic crystals to exhibit second-order nonlinear optical effects which require noncentrosymmetric ordering. The crystal structure of the intensively investigated zwitterionic merocyanine dye **21** was recently resolved by De Ridder et al.[32] As for **1l** and **2c**, a pairwise centrosymmetric packing of the dyes is observed at a distance typical of $\pi-\pi$ contacts (3.49 Å in the central part of the molecule). Due to the high interest in this dye in nonlinear optics, many derivatives have been synthesized, and its zwitterionic character has been established in solution and confirmed by quantum chemical calculations.[39] Upon cocrystallization of two differently substituted derivatives of this dye and a third hydrogen-bond-donating phenol, Bosshard et al. achieved acentric, highly NLO active structures which, however, still preserve an antiparallel

(38) For some examples, see: (a) Cole, J. C.; Howard, J. A. K.; Cross, G. H.; Szablewski, M. *Acta Crystallogr.* **1995**, *C51*, 715−718. (b) Kagawa, H.; Sagawa, M.; Hamada, T.; Kakuta, A.; Kaji, M.; Nakayama, H.; Ishii, K. *Chem. Mater.* **1996**, *8*, 2622−2627. (c) Metzger, R. M.; Heimer, N. E.; Ashwell, G. J. *J. Mol. Cryst. Liq. Cryst.* **1984**, *107*, 133−149. (d) Effenberger, F.; Würthner, F. *Angew. Chem., Int. Ed. Engl.* **1993**, *32*, 719−721. (e) Steybe, F.; Effenberger, F.; Gubler, U.; Bosshard, C.; Günter, P. *Tetrahedron* **1998**, *54*, 8469−8480.

(39) (a) Gruda, I.; Bolduc, F. *J. Org. Chem.* **1984**, *49*, 3300−3305. (b) Niedbalska, M.; Gruda, I. *Can. J. Chem.* **1990**, *68*, 691−695. (c) Morley, J. O.; Morley, R. M.; Docherty, R.; Charlton, M. H. *J. Am. Chem. Soc.* **1997**, *119*, 10192−10202. (d) Morley, J. O.; Morley, R. M.; Fitton, *J. Am. Chem. Soc.* **1998**, *120*, 11479−11488. (e) A. L. Lacroix, P. G.; Daran, J.-C.; Cassoux, P. *New J. Chem.* **1998**, 1085−1091.

orientation of neighboring dyes whose hyperpolarizabilities are, however, not identical anymore.[40]

Intermolecular Interactions. Control of intermolecular forces is of central importance in several disciplines in chemistry, including solid-state chemistry, supramolecular chemistry, and medicinal chemistry. Very often, special terminologies are applied to characterize the respective interactions such as hydrogen-bonding, $\pi-\pi$ stacking, or the hydrophobic effect because of difficulties in separating the different contributions arising from electrostatic interactions, orbital interactions, and dispersion forces.[29,41,42] Especially the nature of $\pi-\pi$ interactions (or $\pi-\pi$ aggregation, $\pi-\pi$ stacking) has been debated for a long time, and quadrupolar interactions (i.e., a negative potential energy surface above the π-system and a positive σ-framework) or dispersion interactions have been favored as the major contributors.[43] On the other hand, the aggregation of π-systems in water, which is ubiquitously found in nature in DNA, protein, and binding of drugs to these molecules but also for small aromatics[44] or self-assembly of charged cyanine[45] and merocyanine dyes,[46] seems to require a different explanation. In this special solvent, the driving force for aggregation seems to arise mainly due to the so-called hydrophobic effect, which is controlled by changes within the microstructure of water around the solute and exhibits a large entropic contribution.[47]

In the following, we will show that none of these complications arises for the merocyanine dyes discussed in this paper and that indeed a very simple electrostatic model accounts for all our observations. We will first analyze the effect of the solvent on the dimerization equilibrium of dye **1a**. In a simple model, two major contributions to the dimerization energy may be identified. The first contribution arises from the interaction of the monomer dipole moment μ_{gM} with the reaction field in the solvent, leading to lowering of the energies of the two monomers relative to the dipoleless dimer. The standard theory of solvatochromism[29,48] treats such effects by approximating the solvent as a dielectric continuum and expressing the polarity on basis of the Kirkwood−Onsager function. The second contribution is due the electrostatic interaction of two interacting monomer dipole moments (Scheme 3) that may be calculated from electrostatic theory within a dielectric with permittivity ϵ_r. The two contributions may be added to yield the following estimate of the Gibbs dimerization energy:

$$\Delta_{dim}G^\circ = \frac{2N_A}{4\pi\epsilon_0 a^3}\left(\frac{(\epsilon_r-1)(\epsilon_r+2)}{9\epsilon_r}\right)\mu_{gM}{}^2 - \frac{N_A}{4\pi\epsilon_0 R^3}\left(\frac{1}{\epsilon_r}\right)\mu_{gM}{}^2(1-3\cos^2\alpha)\sin^3\alpha \quad (15)$$

where a is the Onsager radius of the solvent cavity of the monomer, and the structural parameters of the dimer, the distance R and angle α, have been defined in Scheme 3. The first contribution stabilizes the monomer and the second contribution stabilizes the dimer side of the equilibrium. A fit of the Gibbs dimerization energies for **1a** with two permittivity-dependent functions according to the model eq 15 is shown in Figure 17. An excellent approximation is obtained, which is indeed far better than the fit to any empirical solvent scale,[29] such as $E_T(30)$, Z, or π^*.

The excellent fit is indeed remarkable if we consider that the six solvents tetrachloromethane, trichloroethene, chloroform, butyl acetate, THF, and 1,2-dichloromethane taken into account in this regression exhibit very different features with regard to dispersion interactions (e.g., the chlorinated solvents are here expected to provide much stronger interaction energies) and hydrogen bonding (e.g., THF and butyl acetate are strong hydrogen bond acceptors, whereas chloroform is a weak hydrogen bond donor). However, their influence on electrostatic interactions may be reasonably expressed by means of their macroscopic permittivity, eq 15. In contrast, the microscopic solvent polarity of dioxane and benzene is not correctly

Scheme 3. Model for a Centrosymmetric Dimer of Two Dipolar Dyes[a]

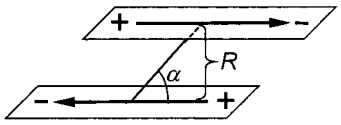

[a] R is the distance between the two π-systems and α is the slip angle that results from the translational offset.

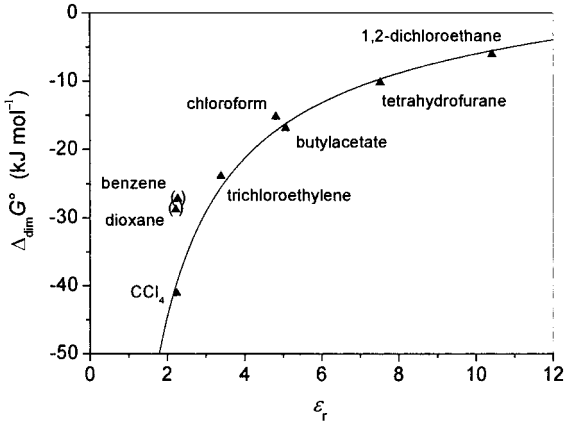

Figure 17. Dependence of the Gibbs dimerization energy of **1a** on the solvent permittivity according to eq 15 and nonlinear regression analysis excluding the data for benzene and dioxane.

(40) (a) Pan, F.; Wong, S.; Gramlich, V.; Bosshard, C.; Günter, P. *J. Am. Chem. Soc.* **1996**, *118*, 6315−6316. (b) Wong, M. S.; Pan, F.; Gramlich, V.; Bosshard, C.; Günter, P. *Adv. Mater.* **1997**, *9*, 554−557.
(41) (a) Israelachvili, J. N. *Intermolecular and Surface Forces*, 2nd ed.; Academic Press: London, 1991. (b) Müller-Dethlefs, K.; Hobza, P. *Chem. Rev.* **2000**, *100*, 143−167. (c) Reed, A. E.; Curtiss, L. A.; Weinhold, F. *Chem. Rev.* **1988**, *88*, 899−926. (d) Morokuma, K. *Acc. Chem. Res.* **1977**, *10*, 294−300.
(42) (a) Schneider, H.-J.; Yatsimirsky, A. K. *Principles and Methods in Supramolecular Chemistry*; J. Wiley & Sons: Chichester, 2000. (b) Steed, J. W.; Atwood, J. L. *Supramolecular Chemistry*; J. Wiley & Sons: Chichester, 2000.
(43) (a) Hunter, C. A.; Sanders, J. K. M. *J. Am. Chem. Soc.* **1990**, *112*, 5525−5534. (b) Hunter, C. A. *Chem. Soc. Rev.* **1994**, 101−109. (c) Hobza, P.; Selzle, H.; Schlag, E. W. *J. Am. Chem. Soc.* **1994**, *116*, 3500−3506. (d) Williams, J. H. *Acc. Chem. Res.* **1993**, *26*, 593−598.
(44) (a) Jorgensen, W. L.; Severance, D. L. *J. Am. Chem. Soc.* **1990**, *112*, 4768−4774. (b) Smithrud, D. B.; Diederich, F. *J. Am. Chem. Soc.* **1990**, *112*, 339−343.
(45) (a) Jelley, E. *Nature* **1936**, *138*, 1009. (b) Scheibe, G. *Z. Angew. Chem.* **1936**, *49*, 563. (c) Herz, A. H. *Adv. Colloid Interface Sci.* **1977**, *8*, 237−298. (d) Möbius, D. *Adv. Mater.* **1995**, *7*, 437−444. (e) Dähne, L. *J. Am. Chem. Soc.* **1995**, *117*, 12855−12860. (f) Von Berlepsch, H.; Böttcher, C.; Dähne, L. *J. Phys. Chem. B* **2000**, *104*, 8792−8799.
(46) (a) Nakahara, H.; Fukuda, K.; Möbius, D.; Kuhn, H. *J. Phys. Chem.* **1986**, *90*, 6144−6148. (b) Mizutani, F.; Iijima, S.; Tsuda, K. *Bull. Chem. Soc. Jpn.* **1982**, *55*, 1295−1299. (c) Kussler, M.; Balli, H. *Helv. Chim. Acta* **1989**, *72*, 17−28.
(47) (a) Murphy, K. P.; Privalov, P. L.; Gill, S. J. *Science* **1990**, *247*, 559−561. (b) Breslow, R. *Acc. Chem. Res.* **1991**, *24*, 159−164. (c) Lemieux, R. U. *Acc. Chem. Res.* **1996**, *29*, 373−380.
(48) Baumann, W. *Physical Methods of Chemistry, Vol. 3B*; Rossiter, B. W., Hamilton, J. F., Eds.; Wiley: New York, 1989; p 45.

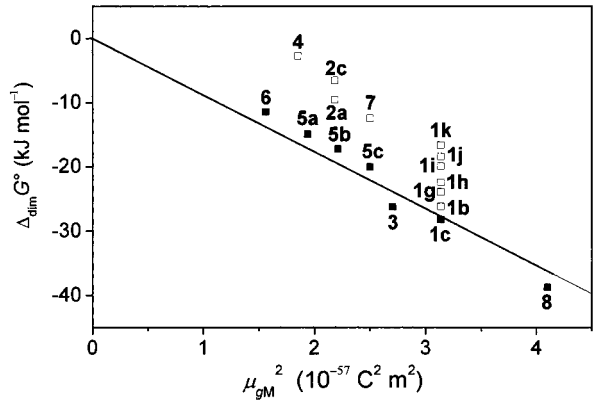

Figure 18. Dependence of the Gibbs dimerization energies measured in dioxane on the dipole moments of the dye molecules (■, □) and linear regression analysis for the solid data points (—).

described by ϵ_r due to the substantial quadrupole moments of the solvent molecules.[48] In the absence of any dipole moment, quadrupole moments become important and may have a significant impact on the dimerization of dye **1a**. Therefore, these two solvents were excluded from the analysis. The excellent fit observed for the remaining solvents strongly supports the electrostatic model of the dimerization process formulated above. From the fit function, eq 15, the Gibbs dimerization energy may be extrapolated to $\Delta_{dim}G° = -90$ kJ mol^{-1} in the gas phase ($\epsilon_r = 1$) and a slip angle of $\alpha = 63°$ is calculated that is close to the value indicated by 2D NMR.

Neglecting the angular dependence of the interaction energy, one expects that the dimerization energy according to eq 15 should be a function of the dipole moment. The dependence of $\Delta_{dim}G°$ on μ_{gM}^2 for merocyanines **1**−**8** (data of Tables 1 and 2) in the same solvent dioxane is displayed in Figure 18.

Indeed, most noncrowded merocyanine dyes (solid squares) lie on a straight line through the origin of the coordinate system. The deviation of a few dyes (open squares) from this behavior may be explained as follows. Dyes **4a**,**b** exhibit a significantly lower dimerization energy because of the strong sterical effect of the 3,3′-dimethylmethylene unit in the central part of the chromophore. To achieve the same reduction of the dimerization energy with regard to the line in Figure 18, tedious synthetic efforts were required for the chromophoric system **1**, which resulted finally in the least aggregating dye of this series, **1k**. This finding underlines the importance of the 3,3-dimethylindoline electron donor unit (also called Fischer's base) in academic as well as industrial cyanine and merocyanine dye chemistry, which is obviously due not only to its strong electron-donating capability but also to its resistance against aggregation. These properties are prerequisites for obtaining dyes with excellent solubility and color brilliance, even at high concentration, in plastics, on textiles, and in other media.[49,50] Two further chromophoric systems, **2** and **7**, exhibit a considerable lower dimerization energy, as suggested by the line. Obviously, their structure deviates from the simple heterocycle−dimethine bridge−heterocycle motif of most of the other dyes of our study. Thus, for dyes **2a**−**d**, the monomethine bridge leads to a bent-shaped chromophore. For such a chromophore, a perfect organization of the whole π-conjugated system on top of each other is possible in a parallel fashion, but not in an antiparallel one (compare crystal structure of **2c**, Figure 10). Accordingly, the contact is not ideal or—speaking in terms of the model of eq 15—the angle α between the two dyes becomes smaller, which should lead to a reduced interaction energy. As for indoline dyes **4**, also for this class of dyes interesting applications arose in the context of photorefractive materials that are again rationalized on the basis of their reduced propensity for aggregation.[34] This allowed high dye loadings and high degrees of poling that led to the most efficient photorefractive gratings known so far. The reduced dimerization energy of dye **7** is tentatively related to the fact that **7** is the only dye without a heterocyclic acceptor. Further studies on such dyes are required to get a more detailed picture of these structurally different chromophores.

Excitonic Coupling. We finally analyze the dimer spectra with respect to the monomer spectra. The interaction of the two subchromophores in the dimer may be understood within an excitonic coupling model based on the point dipole approximation.[51] This model predicts a splitting of the excited energy levels of magnitude

$$hc\Delta\tilde{\nu}_{D21} = hc\left(\frac{1}{\lambda_{D2}} - \frac{1}{\lambda_{D1}}\right) = \frac{2}{4\pi\epsilon_0}\frac{\mu_{agM}^2}{R^3}(1 - 3\cos^2\alpha)\sin^3\alpha \qquad (16)$$

for two identical subchromophores at distance R in the arrangement of Scheme 3, where μ_{agM} is the transition dipole moment of one monomer unit. The model also predicts that the transition to the energetically higher level is intense, with the integrated absorption being twice as large as the one of the monomer band. The transition to the lower level, on the other hand, should be forbidden in the case of an ideal antiparallel arrangement. The predictions of this model are indeed confirmed by the dimer spectra derived from the dilution studies (Figures 1, 4, and 5, and Figures 1−20 in the Supporting Information). The intense dimer band is always observed at shorter wavelength, λ_{D1}, than the monomer band at λ_M. Due to slight deviations from the ideal antiparallel arrangement, the energetically lower transition gains weak intensity and may be observed at longer wavelength, λ_{D2}. This allows calculation of the excitonic splitting, $\Delta\tilde{\nu}_{D21}$, yielding values in the range 3200−3600 cm^{-1} for dyes **1** in Table 1. With the experimentally determined transition dipole moment $\mu_{agM} = 33 \times 10^{-30}$ C m and a splitting energy of about 3200 cm^{-1}, one estimates with eq 16 an angle $\alpha = 60°$, which is in good agreement with the value obtained from eq 15. From the data of Table 2, one concludes that the solvent influence on the excitonic splitting is small. A slight tendency to reduced splittings in more polar solvents may be recognized and tentatively ascribed to a looser structure (larger average value of the distance R) of the dimers in polar environments. Table 3

(49) (a) Raue, R. *Ullmann's Encyclopedia of Industrial Chemistry*, *Vol. 16*, 5th ed.; Elvers, B., Hawkins, S., Schulz, G., Eds.; VCH: Weinheim, 1990; pp 487−529. (b) Tyutyulkov, N.; Fabian, J.; Mehlhorn, A.; Dietz, F.; Tadjer, A. *Polymethine Dyes*; St. Kliment Ohridski University Press: Sofia, 1991.

(50) Grund, C.; Reichelt, H.; Schmidt, A. J.; Würthner, F.; Sens, R.; Beckmann, S. PCT Int. Appl. WO 98/23688, June 4, 1998; *Chem. Abstr.* **1998**, *129*, 29100.

(51) (a) Liptay, W.; Wortmann, R.; Schaffrin, H.; Burkhard, O.; Reitinger, W.; Detzer, N. *Chem. Phys.* **1993**, 120, 429−438. (b) Kasha, M.; Rawls, H. R.; El-Bayoumi, M. A. *Pure Appl. Chem.* **1965**, *11*, 371−392.

Scheme 4. Model for the Competition between External and Internal Forces in the Electric-Field-Induced Poling Process of Dipolar Dyes in Amorphous Composite Materials

collects the observed splittings of the other dyes that lie in the range 1700−3000 cm^{-1}, the lower values (compared to dyes **1**) being mainly caused by the smaller transition dipole moments.

Relevance for Nonlinear Optical Applications of Merocyanine Dyes. Dipolar aggregation of merocyanine dyes is clearly detrimental for the performance of nonlinear optical and photorefractive materials. The experimental and theoretical analyses above demonstrated how the dimerization can be studied quantitatively in liquid solution and how structural variations of the chromophores can be utilized to minimize aggregation. One cannot generally expect that dimerization constants determined in liquid solution can be used to estimate the degree of dimerization in polymers or other glassy solids. However, an estimation of the order of magnitude of the effects in these materials may be feasible. For example, for a polyvinylcarbazole (PVK)-based PR polymer with the chromophore **2d** (called ATOP-1 in our papers on PR materials),[26,34] it was found that for a chromophore content of 40%, about 45% of the chromophore was present in the form of aggregated dimers, and the polarity of PVK was shown to be close to that of DMF.[34] With the known dimerization constant of **2d**, $K_{dim} = 1200\ M^{-1}$ in CCl_4, one may then estimate $K_{dim} \approx 1\ M^{-1}$ in the PR material with eq 15. A **2d** content of 40% corresponds to a concentration of $c_{0M} \approx 1$ M, and it follows from eq 8 that $c_M \approx 0.5$ M, so about 50% of **2d** chromphores would be predicted to be present in the form of dimers, which is in reasonable agreement with the experiment.

Another interesting estimation may be performed with eqs 13 and 14, which express the relative field dependence of the monomer and dimer concentrations. The competition between internal dipole interactions leading to dimerization and external forces leading to dissociation is illustrated in Scheme 4. For **2d**, we have $\mu_{gM} = 44 \times 10^{-30}$ C m (ref 34), and with c_M and c_{0M} as given in the example above, one obtains an electric-field-induced concentration change of $\Delta c_M = 0.05$ M at an externally applied electric field of $E = 60\ V\ \mu m^{-1}$. This is a quite strong shift of the dimerization equilibrium and of major importance for understanding the PR response (as well as second harmonic generation)[52] of materials based on highly dipolar dyes. Since the dimer and monomer differ in their absorption spectra, they also differ in their polarizability, and as a consequence there will be an electric-field-induced increase of the refractive index Δn caused by the field dependence of the dimerization. The absorption maximum of the monomer and dimer of **2d** in the polymer were found to be about 550 and 515 nm, respectively.[26,34] Applying dispersion relations for the linear polarizability and the Clausius−Mosotti equation for the refractive index, one estimates an electric-field-induced index change Δn of the order of 0.001 caused by the field-induced Δc_M at the field strength and conditions specified above. These considerations indicate that electric-field-induced dimer dissociation may significantly contribute to the photorefractive response of organic materials.

(52) A more extended discussion of this topic will be given elsewhere. For earlier work on the influence of dye aggregation on NLO properties of functional polymers, see ref 9.

Conclusion

The dimerization of polar merocyanine dyes in liquid solution was investigated by a combination of several experimental techniques. The formation of centrosymmetric dimer aggregates was concluded from the occurrence of a hypsochromically shifted band in the UV−vis spectra of these chromophores. The concentration and temperature dependence of this band with a clear isobestic point indicated dimerization and allowed determination of Gibbs dimerization energies, enthalpies, and entropies. The optical band shape of the dimer band was explained by an excitonic coupling model assuming antiparallel ordering of two slightly shifted subchromophore dipole moments. This structure was further corroborated by concentration-dependent permittivity measurements, by 2D NMR spectroscopy in liquid solution, and by X-ray crystallography in the solid state. The competition between internal dipole−dipole and external dipole−electric field interactions on the dimerization equilibrium was quantitatively investigated by electrooptical absorption measurements. This effect of an electric field on the dimerization was also estimated for photorefractive organic materials, and it was demonstrated that it may contribute significantly to their nonlinear optical response.

Experimental Section

Solvents and reagents were purchased from Merck unless stated otherwise and purified and dried according to standard procedures.[53] Ethyl isobutyryl acetate **10c**,[54] 2,6-diisopropyl-4-methylpyrylium perchlorate salts **13**,[55] 1-alkyl-4-methylpyridinium bromide **14a**−**c**,**e**,**f**,[56] and *tert*-butyl-4-methylpyridinium perchlorate **14d**[57] were prepared according to literature procedures. **11a**,**c**,**i** were donated by BASF. Typically these hydroxypyridone compounds **11a**−**i** and pyridinium salts **14a**−**i** were used in crude form with the purity determined from NMR analysis. Dyes **1m**, **2**−**8** were prepared as described earlier and purified until C,H,N microanalytical data with a deviation <0.3% were obtained.[14,15,28] Column chromatography was performed on Merck Silica 60 (mesh size 0.2−0.5 mm). NMR spectra were recorded at room temperature on Bruker AC 200, DRX 400, and AMX 500 instruments. Chemical shifts are given in parts per million downfield from TMS as internal standard. All melting points were measured with a Büchi SMP-20 and are uncorrected. The solvents used for UV−vis dilution studies were spectrophotometric grade, purchased from Merck and Aldrich, and used as received. Dioxane for dipole moment measurements was purified by refluxing over sodium under an argon atmosphere and distilled before use. Specific details are given in the text.

General Procedure for the Synthesis of 1,4-Dialkyl-2,6-dioxo-1,2,3,6-tetrahydropyridine-3-carbonitriles 11. Ethyl cyanoacetate (11.31 g, 0.1 mol) was added dropwise to the respective alkylamine (0.25 mol) within 15 min, and stirring was continued at room temperature for 24−48 h to give cyanoacetic acid amides **9a**−**g**. β-Keto acetic acid esters **10a**−**c** (0.1 mol) and piperidine (10 mL) [and NaOH (0.1 mol, 32% aqueous solution) in special cases, i.e., for the synthesis

(53) Perrin, D. D.; Armarego, W. L. F.; Perrin, D. R. *Purification of Laboratory Chemicals*; Pergamon Press: Oxford, 1980; p 77.
(54) Jackman, M.; Klenk, M.; Fishburn, B.; Tullar, B. F.; Archer, S. *J. Am. Chem. Soc.* **1948**, *70*, 2884−2885.
(55) Balaban, A. T.; Nenitzescu, C. D. *Justus Liebigs Ann. Chem.* **1959**, *625*, 74−82.
(56) (a) Coleman, B. D.; Fuoss, R. M. *J. Am. Chem. Soc.* **1955**, *77*, 5472−5476. (b) Morley, J. O.; Morley, R. M.; Docherty, R.; Charlton, M. H. *J. Am. Chem. Soc.* **1997**, *119*, 10192−10202.
(57) Katritzky, A. R.; Rubio, O.; Szajda, M.; Nowak-Wydra, B. *J. Chem. Res. (S)* **1984**, 234−235.

of **11e**,**f**,**h**] were added, and the mixture was stirred at 100 °C for 20 h. The solvent was evaporated, and the pH value was adjusted to 1 with 32% aqueous HCl. After precipitation at room temperature or in the refrigerator, the product was filtered off and washed with water and ether to give a material of sufficient purity (>90%) for further reaction.

1-Dodecyl-4-methyl-2,6-dioxo-1,2,3,6-tetrahydropyridine-3-carbonitrile (11b). Purity, about 98%; yield, 59%. Recrystallization from ethyl acetate gave analytically pure **11b**, mp 164−165 °C. ^{1}H NMR (200 MHz, DMSO): δ 5.62 (1H, s, 5-H), 3.88 (2H, t, J = 7.4 Hz, NCH_2), 2.21 (3H, s, 4-CH_3), 1.52 (2H, m, CH_2), 1.23 (18H, m, CH_2), 0.85 (3H, t, J = 6.4 Hz, CH_3). Anal. Calcd for $C_{19}H_{30}N_2O_2$: C, 71.66; H, 9.50; N, 8.80. Found: C, 71.90; H, 9.70; N, 8.95.

1,4-Dipropyl-2,6-dioxo-1,2,3,6-tetrahydropyridine-3-carbonitrile (11d). Purity, about 99%; yield, 37%. Recrystallization from ethyl acetate/ethanol gave pure **11d**, mp 201−202 °C. ^{1}H NMR (200 MHz, DMSO): δ 5.62 (1H, s, 5-H), 3.86 (2H, t, J = 7.4 Hz, NCH_2), 2.48 (2H, t, J = 7.6 Hz, 4-CH_2), 1.67−1.47 (4H, m, CH_2), 1.23−0.81 (6H, m, CH_3). Anal. Calcd for $C_{12}H_{16}N_2O_2$: C, 65.30; H, 7.37; N, 12.67. Found: C, 65.45; H, 7.37; N, 12.62.

1-Isopropyl-4-propyl-2,6-dioxo-1,2,3,6-tetrahydropyridine-3-carbonitrile (11e). Purity, about 90%; yield, 29%. Recrystallization from ethyl acetate/ethanol gave pure **11e**, mp 213−214 °C. ^{1}H NMR (200 MHz, DMSO): δ 5.59 (1H, s, 5-H), 5.28 (1H, m, NCH), 2.46 (2H, t, J = 7.6 Hz, 4-CH_2), 1.57 (2H, m, CH_2), 1.40 (6H, d, J = 7.1 Hz, $(CH_3)_2$), 0.92 (3H, t, J = 7.2 Hz, CH_3). Anal. Calcd for $C_{12}H_{16}N_2O_2$: C, 65.43; H, 7.32; N, 12.72. Found: C, 65.45; H, 7.37; N, 12.62.

1,4-Diisopropyl-2,6-dioxo-1,2,3,6-tetrahydropyridine-3-carbonitrile (11f). Purity, about 90%; yield, 5%. Recrystallization from ethyl acetate/ethanol gave pure **11f**, mp 226−227 °C. ^{1}H NMR (500 MHz, DMSO): δ 5.58 (1H, s, 5-H), 5.25 (1H, br, NCH), 2.90 (1H, m, 4-CH), 1.38 (6H, d, J = 7.0 Hz, $(CH_3)_2$), 1.14 (6H, d, J = 6.9 Hz, $(CH_3)_2$). Anal. Calcd for $C_{12}H_{16}N_2O_2$: C, 65.43; H, 7.32; N, 12.72. Found: C, 65.45; H, 7.36; N, 12.50.

1-(2-Ethylhexyl)-4-propyl-2,6-dioxo-1,2,3,6-tetrahydropyridine-3-carbonitrile (11g). Purity, about 90%; yield, 23%. Recrystallization from ethyl acetate/ethanol gave pure **11g**, mp 138−139 °C. ^{1}H NMR (200 MHz, DMSO): δ 5.62 (1H, s, 5-H), 3.83 (2H, d, J = 7.4 Hz, NCH_2), 2.49 (2H, m, 4-CH_2), 1.78 (1H, m, CH), 1.58 (2H, m, CH_2), 1.22 (8H, m, CH_2), 0.87 (9H, m, CH_3). Anal. Calcd for $C_{17}H_{26}N_2O_2$: C, 70.31; H, 9.02; N, 9.65. Found: C, 70.22; H, 9.01; N, 9.69.

1-(1-Methylbutyl)-4-propyl-2,6-dioxo-1,2,3,6-tetrahydropyridine-3-carbonitrile (11h). Purity, about 90%; yield, 19%. Recrystallization from ethyl acetate gave pure **12h**, mp 176−177 °C. ^{1}H NMR (500 MHz, DMSO): δ 5.55 (1H, s, 5-H), 5.26 (1H, br, NCH), 2.45 (2H, m, 4-CH_2), 1.82 (1H, br, CH_2), 1.65 (1H, m, CH_2), 1.56 (2H, m, CH_2), 1.36 (3H, d, J = 5.1 Hz, CH_3), 1.14 (2H, m, CH_2), 0.91 (3H, t, J = 7.4 Hz, CH_3), 0.83 (3H, t, J = 7.4 Hz, CH_3). Anal. Calcd for $C_{14}H_{20}N_2O_2$: C, 67.72; H, 8.12; N, 11.28. Found: C, 67.91; H, 7.98; N, 11.31.

General Procedure for the Synthesis of 1-Alkyl-2,6-diisopropyl-4-methylpyridinium Perchlorate Salts 14g,h. To a stirred suspension of 2,6-diisopropyl-4-methylpyrylium perchlorate (5.25 g, 0.02 mol) and the respective alkylamine (0.022 mol) in dry dichloromethane (150 mL) was added triethylamine (6.1 g, 0.06 mol) dropwise in 15 min. The resulting solution was stirred for 20 h at room temperature and then poured into a separatory funnel, where it was washed with aqueous HCl (10%, 20 mL) and water (40 mL). The organic phase was dried over anhydrous sodium sulfate and concentrated in a rotary evaporator until almost all solvent was removed. Diethyl ether was added (40 mL), and the precipitated pyridinium salt was separated by filtration and dried to give the crude product.

1-Propyl-2,6-diisopropyl-4-methylpyridinium Perchlorate (14h). Purity, about 95%; yield, 51%. Recrystallization from EtOH afforded pure **14h**, mp 150−151 °C. ^{1}H NMR (200 MHz, $CDCl_3$): δ 7.56 (2H, s, pyridine-3,5-H), 4.49 (2H, t, J = 8.6 Hz, NCH_2), 3.44 (2H, m, CH), 2.63 (3H, s, 4-CH_3), 1.85 (2H, m, CH_2), 1.47 (12H, d, J = 6.4 Hz, $(CH_3)_2$), 1.14 (3H, t, J = 7.4 Hz, CH_3). Anal. Calcd for $C_{15}H_{27}NClO_4$: C, 56.15; H, 8.49; N, 4.37. Found: C, 56.49; H, 8.20; N, 4.30.

1-Dodecyl-2,6-diisopropyl-4-methylpyridinium Perchlorate (14g). Purity, about 75%; yield, 62%; used without further purification. ^{1}H NMR (400 Hz, $CDCl_3$): δ 7.53 (2H, s, pyridine-3,5-H), 4.50 (2H, t, J = 8.4 Hz, NCH_2), 3.41 (2H, m, CH), 2.62 (3H, s, 4-CH_3), 1.80 (2H, m, CH_2), 1.47 (12H, d, J = 6.4 Hz, $(CH_3)_2$), 1.25 (18H, m, CH_2), 0.87 (3H, t, J = 6.4 Hz, CH_3).

Synthesis of 1-Hexyl-4-methyl-2,6-dioxo-5-phenyliminomethylene-1,2,5,6-tetrahydropyridine-3-carbonitrile (15a). Hexyl pyridone **11a** (11.70 g, 50 mmol) and *N*,*N*′-diphenylformamidine (9.82 g, 50 mmol) in dry Ac_2O (40 mL) were stirred at room temperature until the mixture solidified. To complete the reaction, the mixture was heated at 80−90 °C for 15 min. The precipitate obtained upon cooling was filtered off, washed with MeOH, and dried in vacuo to give pure **15a** (14.2 g, 84%), mp 181−182 °C. ^{1}H NMR (200 MHz, $CDCl_3$): δ 13.13 (1H, d, J = 13.8 Hz, NH), 8.19 (1H, d, J = 12.8 Hz, methine-H), 7.48 (2H, m, phenyl-H), 7.29 (3H, m, phenyl-H), 3.98 (2H, t, J = 7.4 Hz, NCH_2), 2.53 (3H, s, pyridone-4-CH_3), 1.60 (2H, m, CH_2), 1.33 (6H, m, CH_2), 0.89 (3H, t, J = 6.9 Hz, CH_3). Anal. Calcd for $C_{20}H_{23}N_3O_2$: C, 71.19; H, 6.87; N, 12.45. Found: C, 70.98; H, 6.86; N, 12.45.

General Procedure for the Synthesis of Dyes 1a−m. A pyridone **11a−i** (4 mmol) and *N*,*N*′-diphenylformamidine (4 mmol) in Ac_2O (4 mL) were stirred at room temperature until the mixture solidified. The mixture was heated at 80−90 °C for 15 min to complete the reaction. After the reaction mixture cooled to room temperature, a pyridinium salt **14a−i** (4 mmol) and KOAc (4 mmol) were added, and the mixture was heated at 90 °C for another 2 h. The solution was concentrated in vacuo, and the crude product was purified by column chromatography on silica using dichloromethane/methanol 95:5 or ethyl acetate/toluene 1:1 as eluent. Recrystallization from acetic acid, toluene, or ethanol/hexane gave pure dyes **1a−m**.

1-Dodecyl-4-methyl-2,6-dioxo-5-[2-(1-dodecyl-1-hydropyridin-4-ylidene)ethylidene]-1,2,5,6-tetrahydropyridine-3-carbonitrile (1a). Yield, 90%; mp 154−156 °C. ^{1}H NMR (200 MHz, $CDCl_3$): δ 7.74 (1H, d, J = 15.3 Hz, methine-H), 7.63 (2H, d, J = 6.9 Hz, pyridine-2,6-H), 7.47 (1H, d, J = 14.8 Hz, methine-H), 7.20 (2H, d, J = 6.9 Hz, pyridine-3,5-H), 4.19 (2H, t, J = 7.4 Hz, pyridine-NCH_2), 3.94 (2H, t, J = 7.6 Hz, pyridone-NCH_2), 2.27 (3H, s, pyridone-4-CH_3), 1.90 (2H, m, CH_2), 1.63 (2H, m, CH_2), 1.29 (36H, m, CH_2), 0.87 (6H, m, CH_3). Anal. Calcd for $C_{38}H_{59}N_3O_2$: C, 77.37; H, 10.08; N, 7.12. Found: C, 77.23; H, 10.10; N: 7.12.

1-(2-Ethylhexyl)-4-methyl-2,6-dioxo-5-[2-(1-(2-ethylhexyl)-1-hydropyridin-4-ylidene)ethylidene]-1,2,5,6-tetrahydropyridine-3-carbonitrile (1b). Yield, 89%; mp 177−179 °C. ^{1}H NMR (200 MHz, $CDCl_3$): δ 7.74 (1H, d, J = 14.8 Hz, methine-H), 7.59 (1H, d, J = 14.8 Hz, methine-H), 7.57 (2H, d, J = 8.4 Hz, pyridine-2,6-H), 7.24 (2H, d, J = 8.4 Hz, pyridine-3,5-H), 4.05 (2H, d, J = 7.4 Hz, pyridine-NCH_2), 3.91 (2H, m, pyridone-NCH_2), 2.32 (3H, s, pyridone-4-CH_3), 1.81 (2H, m, CH), 1.40−1.29 (16H, m, CH_2), 0.98−0.85 (12H, m, CH_3). ^{13}C NMR (125 MHz, THF-d_8; HMQC, HMBC): δ 164.3 (C═O), 163.6 (C═O), 157.8 (q, pyridine-4-C), 156.0 (C), 141.9 (pyridine-2,6-CH), 141.0 (methine-CH), 120.2 (pyridine-3,5-CH), 119.4 (CN), 113.4 (methine-CH), 107.0 (C), 89.7 (C), 62.8 (pyridine-NCH_2), 43.3 (NCH_2), 41.7 (CH), 38.6 (CH), 31.9 (CH_2), 30.8 (CH_2), 29.7 (CH_2), 29.2 (CH_2), 25.8 (CH_2), 24.9 (CH_2), 24.1 (CH_2), 23.8 (CH_2), 18.5 (CH_3), 14.5 (CH_3), 14.3 (CH_3), 11.1 (CH_3), 10.6 (CH_3). Anal. Calcd for $C_{30}H_{43}N_3O_2$: C, 75.43; H, 9.07; N, 8.80. Found: C, 75.12; H, 8.80; N, 8.84.

1-Hexyl-4-methyl-2,6-dioxo-5-[2-(1-hexyl-1-hydropyridin-4-ylidene)ethylidene]-1,2,5,6-tetrahydropyridine-3-carbonitrile (1c). Yield, 90%; mp 165−166 °C. ^{1}H NMR (200 MHz, $CDCl_3$): δ 7.75 (1H, d, J = 14.8 Hz, methine-H), 7.62 (2H, d, J = 6. 9 Hz, pyridine-2,6-H), 7.50 (1H, d, J = 14.8 Hz, methine-H), 7.21 (2H, d, J = 6. 9 Hz, pyridine-3,5-H), 4.18 (2H, t, J = 7.6 Hz, pyridine-NCH_2), 3.95 (2H, t, J = 7.6 Hz, pyridone-NCH_2), 2.29 (3H, s, pyridone-4-CH_3), 1.91 (2H, m, CH_2), 1.59 (2H, m, CH_2), 1.34 (12H, m, CH_2), 0.89 (6H,

m, 2CH_3). Anal. Calcd for $C_{26}H_{35}N_3O_2$: C, 74.07; H, 8.37; N, 9.97. Found: C, 74.08; H, 8.41; N, 9.95.

1-Hexyl-4-methyl-2,6-dioxo-5-[2-(1-butyl-1-hydropyridin-4-yl-idene)ethylidene]-1,2,5,6-tetrahydropyridine-3-carbonitrile (1d). Yield, 64%; mp 103−104 °C. ^{1}H NMR (200 MHz, $CDCl_3$): δ 7.74 (1H, d, J = 14.8 Hz, methine-H), 7.64 (2H, d, J = 7.4 Hz, pyridine-2,6-H), 7.48 (1H, d, J = 14.8 Hz, methine-H), 7.20 (2H, d, J = 7.4 Hz, pyridine-3,5-H), 4.19 (2H, t, J = 7.4 Hz, pyridine-NCH_2), 3.95 (2H, t, J = 7.6 Hz, pyridone-NCH_2), 2.28 (3H, s, pyridone-4-CH_3), 1.90 (2H, m, CH_2), 1.63 (2H, m, CH_2), 1.33−1.51 (m, 8H, CH_2), 1.00 (3H, t, J = 7.1 Hz, CH_3), 0.88 (3H, t, J = 6.9 Hz, CH_3). Anal. Calcd for $C_{24}H_{31}N_3O_2$: C, 73.25; H, 7.94; N, 10.68. Found: C, 73.00; H, 7.88; N, 10.55.

1-Hexyl-4-methyl-2,6-dioxo-5-[2-(1-isobutyl-1-hydropyridin-4-ylidene)ethylidene]-1,2,5,6-tetrahydropyridine-3-carbonitrile (1e). Yield, 75%; mp 207−209 °C. ^{1}H NMR (200 MHz, $CDCl_3$): δ 7.78 (1H, d, J = 14.8 Hz, methine-H), 7.75 (2H, d, J = 6.9 Hz, pyridine-2,6-H), 7.59 (1H, d, J = 14.8 Hz, methine-H), 7.30 (2H, d, J = 6.9 Hz, pyridine-3,5-H), 4.13 (1H, m, pyridine-NCH), 3.95 (2H, t, J = 7.6 Hz, pyridone-NCH_2), 2.37 (3H, s, pyridone-4-CH_3), 1.93 (2H, m, CH_2), 1.60−1.69 (5H, m, CH_2 and CH_3), 1.32 (6H, m, CH_2), 0.84−0.99 (6H, m, CH_3). Anal. Calcd for $C_{24}H_{31}N_3O_2$: C, 73.25; H, 7.94; N, 10.68. Found: C, 73.18; H, 8.01; N, 10.60.

1-Hexyl-4-methyl-2,6-dioxo-5-[2-(1-*tert*-butyl-1-hydropyridin-4-ylidene)ethylidene]-1,2,5,6-tetrahydropyridine-3-carbonitrile (1f). Yield, 79%; mp 253−254 °C. ^{1}H NMR (200 MHz, DMSO): δ 8.66 (2H, d, J = 7.1 Hz, pyridine-2,6-H), 7.81 (1H, d, J = 15.3 Hz, methine-H), 7.79 (2H, d, J = 7.1 Hz, pyridine-3,5-H), 7.72 (1H, d, J = 15.0 Hz, methine-H), 3.81 (2H, t, J = 7.3 Hz, pyridone-NCH_2), 2.41 (3H, s, pyridone-4-CH_3), 1.67 (9H, s, $(CH_3)_3$), 1.46 (2H, m, CH_2), 1.26 (6H, m, CH_2), 0.86 (3H, t, J = 6.4 Hz, CH_3). Anal. Calcd for $C_{24}H_{31}N_3O_2$: C, 73.25; H, 7.94; N, 10.68. Found: C, 73.17; H, 7.90; N, 10.62.

1,4-Dipropyl-2,6-dioxo-5-[2-(1-*sec*-butyl-1-hydropyridin-4-ylidene)ethylidene]-1,2,5,6-tetrahydropyridine-3-carbonitrile (1g). Yield, 32%; mp 254−256 °C. ^{1}H NMR (200 MHz, $CDCl_3$): δ 8.03 (2H, d, J = 7.4 Hz, pyridine-2,6-H), 7.89 (1H, d, J = 14.8 Hz, methine-H), 7.70 (1H, d, J = 14.8 Hz, methine-H), 7.44 (2H, d, J = 6.9 Hz, pyridine-3,5-H), 4.31 (1H, m, pyridine-NCH), 3.96 (2H, m, pyridone-NCH_2), 2.81 (2H, t, J = 7.6 Hz, pyridone-4-CH_2), 1.96 (2H, m, CH_2), 1.57−1.87 (7H, m, CH_2 and CH_3), 1.06 (3H, t, J = 7.4 Hz, CH_3), 0.89−0.99 (6H, m, CH_3). Anal. Calcd for $C_{23}H_{29}N_3O_2$: C, 72.79; H, 7.70; N, 11.07. Found: C, 72.73; H, 7.67; N, 11.02.

1-Isopropyl-4-propyl-2,6-dioxo-5-[2-(1-*sec*-butyl-1-hydropyridin-4-ylidene)ethylidene]-1,2,5,6-tetrahydropyridine-3-carbonitrile (1h). Yield, 56%; mp 274−275 °C. ^{1}H NMR (200 MHz, $CDCl_3$): δ 7.93 (2H, d, J = 6.4 Hz, pyridine-2,6-H), 7.83 (1H, d, J = 14.8 Hz, methine-H), 7.69 (1H, d, J = 14.3 Hz, methine-H), 7.40 (2H, d, J = 6.9 Hz, pyridine-3,5-H), 5.37 (1H, m, pyridone-NCH), 4.26 (1H, m, pyridine-NCH), 2.78 (2H, t, J = 7.6 Hz, pyridone-4-CH_2), 1.93 (2H, m, CH_2), 1.62−1.72 (5H, m, CH_2 and CH_3), 1.48 (6H, m, $(CH_3)_2$), 1.06 (3H, t, J = 7.1 Hz, CH_3), 0.94 (3H, t, J = 7.4 Hz, CH_3). Anal. Calcd for $C_{23}H_{29}N_3O_2$: C, 72.79; H, 7.70; N, 11.07. Found: C, 72.59; H, 7.65; N, 10.97.

1,4-Diisopropyl-2,6-dioxo-5-[2-(1-*sec*-butyl-1-hydropyridin-4-ylidene)ethylidene]-1,2,5,6-tetrahydropyridine-3-carbonitrile (1i). Yield, 55%; mp 121−123 °C. ^{1}H NMR (200 MHz, $CDCl_3$): δ 7.97 (1H, d, J = 14.3 Hz, methine-H), 7.89 (2H, d, J = 7.4 Hz, pyridine-2,6-H), 7.83 (1H, d, J = 14.8 Hz, methine-H), 7.40 (2H, d, J = 6.9 Hz, pyridine-3,5-H), 5.37 (1H, m, pyridone-NCH), 4.25 (1H, m, pyridine-NCH), 3.55 (1H, m, pyridone-4-CH), 1.92 (2H, m, CH_2), 1.62 (3H, d, J = 6.4 Hz, CH_3), 1.47 (12H, m, $(CH_3)_2$), 0.94 (3H, t, J = 7.4 Hz, CH_3). Anal. Calcd for $C_{23}H_{29}N_3O_2$: C, 72.79; H, 7.70; N, 11.07. Found: C, 72.50; H, 7.77; N, 10.77.

1-(2-Ethylhexyl)-4-propyl-2,6-dioxo-5-[2-(1-dodecyl-2,6-diisopropyl-1-hydropyridin-4-ylidene)ethylidene]-1,2,5,6-tetrahydropyridine-3-carbonitrile (1j). Isolated by freeze-drying from dioxane; yield, 63%; mp 105−108 °C. ^{1}H NMR (200 MHz, $CDCl_3$): δ 7.80 (1H, d, J = 14.8 Hz, methine-H), 7.68 (1H, d, J = 14.8 Hz, methine-H), 7.21 (2H, s, pyridine-H), 4.11 (2H, t, J = 8.1 Hz, pyridine-NCH_2), 3.95 (2H, m, pyridone-NCH_2), 3.18 (2H, m, CH), 2.84 (2H, t, J = 7.9 Hz, pyridone-4-CH_2), 1.94 (1H, m, CH), 1.70 (4H, m, CH_2), 1.41 (12H, d, J = 6.4 Hz, $(CH_3)_2$), 1.27 (26H, m, CH_2), 1.08 (3H, t, J = 7.1 Hz, CH_3), 0.87 (9H, m, CH_3). HRMS (EI, 70 eV): M^+ 646.5305 (calcd 646.5312). Anal. Calcd for $C_{42}H_{67}N_3O_2$: C, 78.09; H, 10.45; N, 6.50. Found: C, 77.40; H, 10.45; N, 6.30.

1-(1-Methylbutyl)-4-propyl-2,6-dioxo-5-[2-(1-dodecyl-2,6-diisopropyl-1-hydropyridin-4-ylidene)ethylidene]-1,2,5,6-tetrahydropyridine-3-carbonitrile (1k). Yield, 52%; mp 160−162 °C. ^{1}H NMR (500 MHz, $CDCl_3$): δ 7.75 (1H, d, J = 14.7 Hz, methine-H), 7.68 (1H, d, J = 14.7 Hz, methine-H), 7.19 (2H, s, pyridine-H), 5.23 (1H, m, pyridone-NCH), 4.11 (2H, m, pyridine-NCH_2), 3.16 (2H, m, CH), 2.81 (2H, m, pyridone-4-CH_2), 2.10 (1H, br, CH), 1.94 (1H, m, CH), 1.70 (4H, m, CH_2), 1.47 (3H, m, CH_3), 1.40 (12H, d, J = 6.5 Hz, $(CH_3)_2$), 1.27 (20H, m, CH_2), 1.08 (3H, t, J = 7.35 Hz, CH_3), 0.88 (6H, m, CH_3). Anal. Calcd for $C_{39}H_{61}N_3O_2$: C, 77.56; H, 10.18; N, 6.96. Found: C, 77.94; H, 10.49; N, 7.00.

1-Isopropyl-4-propyl-2,6-dioxo-5-[2-(1-propyl-2,6-diisopropyl-1-hydropyridin-4-ylidene)ethylidene]-1,2,5,6-tetrahydropyridine-3-carbonitrile (1l). Yield, 67%; mp 277−278 °C. ^{1}H NMR (200 MHz, $CDCl_3$): δ 7.77 (1H, d, J = 14.8 Hz, methine-H), 7.67 (1H, d, J = 14.8 Hz, methine-H), 7.19 (2H, s, pyridine-H), 5.40 (1H, m, pyridone-NCH), 4.08 (2H, t, J = 8.4 Hz, pyridine-NCH_2), 3.16 (2H, m, CH), 2.81 (2H, t, J = 7.6 Hz, pyridone-4-CH_2), 1.71 (4H, m, CH_2), 1.51 (6H, d, J = 6.9 Hz, CH_3), 1.41 (12H, d, J = 6.9 Hz, $(CH_3)_2$), 1.15−1.05 (6H, m, CH_3). Anal. Calcd for $C_{28}H_{39}N_3O_2$: C, 74.80; H, 8.74; N, 9.35. Found: C, 74.68; H, 8.88; N, 9.30.

3,4-Diethylthiophene (17). At room temperature and under an argon atmosphere, 0.1 mol of ethylmagnesium bromide in 30 mL of ether was added dropwise into a mixture of 9.40 g (0.039 mol) of 3,4-dibromothiophene **16**, 217 mg (0.4 mmol) of $NiCl_2$dppp, and 15 mL of anhydrous ether, and the mixture was refluxed for 24 h. The resulting solution was hydrolyzed with 40 mL of 1 N HCl and 100 mL of ice−water. The organic layer and ether extracts from the aqueous layer were combined, washed with water, and dried over Na_2SO_4. After evaporation of the solvent, vacuum distillation afforded 3.8 g of **17** at 80 °C/11 mbar (ref 58: 70 °C/12 Torr); yield, 70%.

2,5-Dibromo-3,4-diethylthiophene (18). To 17.0 g (0.12 mol) of 3,4-diethylthiophene **17** in 200 mL of a 50:50 (v/v) mixture of chloroform and acetic acid was added 47.0 g (0.26 mol) of *N*-bromosuccinimide (NBS). The mixture was stirred at room temperature for 1 h and at 70 °C for another 4 h. The mixture was poured into ice−water and extracted with dichloromethane. The combined organic extracts were washed with water, 10% $NaHCO_3$ (twice), and again with water and dried over Na_2SO_4. Removal of the solvent afforded 32.05 g of **18** at a purity of 95% (from NMR); yield, 90%. ^{1}H NMR (200 MHz, $CDCl_3$): δ = 2.59 (q, 4H, J = 7.6 Hz, CH_2), 1.11 (t, 3H, J = 7.6 Hz, CH_3).

2-Bromo-3,4-diethyl-5-formylthiophene (19). A 2.56-mL (6.0 mmol) portion of a 15% solution of butyllithium in hexane was slowly (1 h) added to 1.68 g (95%, 5.7 mmol) of 3,4-diethyl-2,5-dibromothiophene **18** in 20 mL of dry ether under argon atmosphere at −70 °C and warmed to − 50 °C. Next, 0.52 mL (7.2 mmol) of DMF was added dropwise and the mixture allowed to warm to room temperature overnight. The mixture was poured into 1 mL of 12 M HCl in ice−water and extracted with ether. The organic layers were combined, washed with water, and dried over Na_2SO_4. Removal of the solvent left 1.22 g (purity 90% from NMR); yield, 78%. Recrystallization from toluene/hexane afforded pure **19**, mp 58−59 °C. ^{1}H NMR (200 MHz, $CDCl_3$): δ 9.93 (1H, s, CHO), 2.93 (2H, q, J = 7.6 Hz, CH_2), 2.62

(58) Boelens, H.; Branksma, L. *Recl. Trav. Chim. Pays-Bas* **1972**, *91*, 141−144.

(2H, q, $J = 7.6$ Hz, CH_2), 1.26 (3H, t, $J = 7.6$ Hz, CH_3), 1.14 (3H, t, $J = 7.6$ Hz, CH_3). Anal. Calcd for $C_9H_{11}BrOS$: C, 43.74; H, 4.49; S, 12.97. Found: C, 43.67; H, 4.44; S, 13.09.

1-Butyl-5-[5-*N*-butyl-*N*-ethylamino)-3,4-diethylthiophen-2-ylmethylene]-4-methyl-2,6-dioxo-1,2,5,6-tetrahydropyridine-3-carbonitrile (2c). A 1.24-g (90% purity, 4.5 mmol) amount of thiophene carbaldehyde **19**, 1.51 g (15.0 mmol) of ethylbutylamine, and 0.1 g of toluene-4-sulfonic acid were mixed and stirred at a bath temperature of 100 °C for 20 h. The mixture was cooled, and 25 mL of water was added. The organic layer and dichloromethane extracts were combined, washed with water, and dried over $MgSO_4$. The solvent was removed, and the residue was dried under vacuum to give crude **20**. This material was mixed with 0.93 g (4.5 mmol) of **11i** and 6 mL of acetic anhydride and heated at 100 °C for 1 h. Evaporation of the solvent, purification by chromatography (silica, dichloromethane/methanol 96:4), and recrystallization from ethanol/hexane afforded 0.47 g of a red solid; yield, 23%; mp 146−147 °C. ^{1}H NMR (200 MHz, $CDCl_3$): δ 7.77 (1H, s, methine-H), 3.98 (2H, t, $J = 7.63$ Hz, NCH_2), 3.75−3.56 (4H, m, NCH_2), 2.79 (2H, m, CH_2), 2.62 (2H, m, CH_2), 2.49 (3H, s, CH_3), 1.73 (2H, m, CH_2), 1.60 (2H, m, CH_2), 1.55−1.33 (10H, m, CH_2), 1.01−0.88 (6H, m, CH_3). Anal. Calcd for $C_{26}H_{37}N_3O_2S$ (455.7): C, 68.53; H, 8.18; N, 9.22; S, 7.04. Found: C, 68.37; H, 8.08; N, 9.21; S, 6.79.

UV−Vis Absorption Studies. The UV−vis absorption spectra were recorded at 20 °C with a Perkin-Elmer Lambda 40P UV−vis spectrometer, using matched silica cells of 0.001−5.0 cm path length to cover a suitable concentration range. The spectral bandwidth and the scan speed were 1.0 nm and 60 or 120 nm/min. The stock solutions of each compound were accurately prepared, and dilutions of these stocks were used for absorption measurements over a concentration range taking into account solubility and absorbance. In the case of temperature-dependent studies, the temperature was controlled with a deviation of ±0.1 °C within the cell by circulating a mixture of water/ethylene glycol 1:1 from a Braun Melsungen thermomix 1440 thermoregulator.

Dipole Moment Studies. The solutions were prepared by accurately weighing appropriate amounts of solute in 50-mL volumetric flasks and then adding solvent to reach the 50-mL mark. The dielectric constants of the solutions were measured by a WTW Dipolmeter DM01 using a thermostated MFL1 cylindrical condenser cell. The refractive indices were determined by the use of a Bausch and Lomb Abbe-3L refractometer. The temperature of the experiment was 25.0 ± 0.1 °C. The temperature control for both the dipole meter and the refractometer was achieved by circulating a mixture of water/ethyleneglycol 1:1 from a thermoregulator, MGW LAUDA RM6.

Electrooptical Absorption Measurements (EOAM). EOAM experiments were performed as previously described.[17a,b] The measurements were carried out with dioxane, which was purified and carefully dried by distillation from Na/K under argon prior to use. The absorbances of the solutions were determined with a Perkin-Elmer Lambda 900 spectrophotometer.

Crystal Structure Determination of Dye 1l. Green shining prism crystals of dye **1l** were grown slowly in an ethanol/hexane dye solution at −18 °C. The crystal investigated by XRD (crystal size 0.19 × 0.23 × 0.69 mm) belongs to the triclinic system with cell dimensions $a = 9.660(2)$ Å, $b = 11.339(2)$ Å, $c = 13.084(2)$ Å, $\alpha = 71.00(2)°$, $\beta = 78.85(2)°$, $\gamma = 78.94(2)°$, and $V = 1316.6(4)$ Å^3. The space group is $P\bar{1}$ (IT No. 2) and $Z = 2$. The empirical formula is $C_{28}H_{39}N_3O_2$, the molar mass is $M_r = 449.62$, and the calculated density is $\rho_{calcd} = 1.134$ g cm^{-3}. The three-dimensional X-ray data were collected at 220 K with graphite-monochromated Mo Kα radiation ($\lambda = 71.073$ pm) using a STOE-IPDS diffractometer, in the range $2\theta_{min} = 1.61°$ to $2\theta_{max} = 24.07°$, scan modus rotation. The intensity data of 8368 independent reflexes were collected; 3876 unique reflections ($|I^0| > 2\sigma|I^0|$) were used in the analysis (residual electron density +0.151/−0.265 e Å^{-3}). The structure was solved by direct methods (program XMY93)[59a] and refined on F^2 using the full-matrix least-squares method of SHELXL 97.[59b] No absorption correction (0.071 mm^{-1}) was done. Hydrogen atoms were obtained from a final difference Fourier map and included in the refinement. Non-hydrogen atoms were assigned anisotropic and hydrogen atoms isotropic temperature factors, converging to a final R factor of 0.0522 and a weighted R factor of 0.1188 ($w = 1/[\sigma^2(F_o^2) + (0.0642P)^2]$), where $P = (F_o^2 + 2F_c^2)/3$.

Crystal Structure Determination of Dye 2c. Green shining prism crystals of dye **2c** were grown slowly in an ethanol/hexane dye solution at −18 °C. The crystal investigated by XRD (crystal size 0.11 × 0.22 × 0.46 mm) belongs to the monoclinic system with cell dimensions of $a = 8.574(1)$ Å, $b = 23.833(2)$ Å, $c = 12.382(1)$ Å, $\beta = 98.27(1)°$, and $V = 2503.8(3)$ Å^3. The space group is $P2_1$ (IT No. 4) and $Z = 4$. The empirical formula is $C_{26}H_{37}N_3O_2S$, the molar mass is $M_r = 455.65$, and the calculated density is $\rho_{calcd} = 1.209$ g cm^{-3}. The three-dimensional X-ray data were collected at 173 K with graphite-monochromated Mo Kα radiation ($\lambda = 71.073$ pm) in the range from $2\theta_{min} = 0.34°$ to $2\theta_{max} = 24.15°$, using a STOE-IPDS diffractometer. The intensity data of 18 814 reflections were collected, with 7865 unique reflections (with $|I^0| > 2\sigma|I^0|$), and were used in the analysis (residual electron density +0.493/−0.373 e Å^{-3}). The structure was solved by direct methods (program XMY93)[59a] and refined on F^2 using the full-matrix least-squares method of SHELXL 97.[59b] No absorption correction was done (0.156 mm^{-1}). Hydrogen atoms were included in the refinement by using a riding model. Non-hydrogens atoms were assigned anisotropic and hydrogen atoms isotropic temperature factors, converging to a final R factor of 0.0485 and a weighted R factor of 0.1131 ($w = 1/[\sigma^2(F_o^2) + (0.0642P)^2]$), where $P = (F_o^2 + 2F_c^2)/3$.

2D NMR Spectroscopy. Measurements were made in standard 5-mm NMR tubes at 300 K. Prior to two-dimensional NMR measurements, the samples were degassed by bubbling with dry argon for at least 30 min. Two-dimensional ROE spectra were recorded with a standard pulse sequence over a sweep width of 3205 Hz using 2048 data points in the t_2 dimension and 512 increments in the t_1 dimension with different mixing times $\tau_{m1} = 400$ ms and $\tau_{m2} = 300$ ms. A total of 160 scans were collected for each t_1 increment to achieve sufficient sensitivity and resolution, and the repetition delay was 3.0 s. The spectra were acquired at low mixing times (300 ms) to differentiate between ROE connectivities and chemical exchange peaks. A spectral width of 6097 Hz was used in both dimensions, containing 2048 and 256 data points.

Differential Scanning Calorimetry (DSC). DSC measurements were performed on a Perkin-Elmer DSC 7 instrument with heating and cooling rates of 10 K min^{-1}.

Acknowledgment. This work was supported by the Deutsche Forschungsgemeinschaft (research grants Wu 317/1-2 and Wu 317/1-3) and BASF AG (travel grant for S.Y.). We thank Dr. Udo Werz for carrying out the 2D NMR measurements and Christopher Klein, Mesfin Redi-Abshiro, and Christian Schmitz for performing EOAM measurements.

Supporting Information Available: Concentration-dependent UV−vis spectra for dyes **1**−**8** in dioxane and **1a** in various solvents; tables of atomic positional parameters, bond distances, bond angles, anisotropic thermal parameters, hydrogen atom positions, and data collection parameters of the single-crystal X-ray structure determinations of **1l** and **2c** (PDF). This material is available free of charge via the Internet at http://pubs.acs.org.

JA020168F

(59) (a) Debaerdemaeker, T. *XMY93 Program*; University of Ulm, Germany, 1993. (b) Sheldrick, G. M. *SHELXL-97*, Program for the Refinement of Crystal Structures; Univeristy of Göttingen, Germany, 1997.